
NSNQuant: A Double Normalization Approach for Calibration-Free Low-Bit Vector Quantization of KV Cache

Donghyun Son
Seoul National University
happydh1@snu.ac.kr

Euntae Choi
Seoul National University
euntae.choi175@gmail.com

Sungjoo Yoo*
Seoul National University
sungjoo.yoo@gmail.com

Abstract

Large Language Model (LLM) inference is typically memory-intensive, especially when processing large batch sizes and long sequences, due to the large size of key-value (KV) cache. Vector Quantization (VQ) is recently adopted to alleviate this issue, but we find that the existing approach is susceptible to distribution shift due to its reliance on calibration datasets. To address this limitation, we introduce **NSNQuant**, a calibration-free Vector Quantization (VQ) technique designed for low-bit compression of the KV cache. By applying a three-step transformation—**1**) a token-wise normalization (**Normalize**), **2**) a channel-wise centering (**Shift**), and **3**) a second token-wise normalization (**Normalize**)—with Hadamard transform, NSNQuant effectively aligns the token distribution with the standard normal distribution. This alignment enables robust, calibration-free vector quantization using a single reusable codebook. Extensive experiments show that NSNQuant consistently outperforms prior methods in both 1-bit and 2-bit settings, offering strong generalization and up to $3\times$ throughput gain over full-precision baselines.

1 Introduction

Large language models (LLMs) have been widely adopted across various domains due to their strong generalization capabilities [1]. Recently, with the emerging trend of using LLMs to solve complex problems, their use has expanded into long-context scenarios such as long-context reasoning [40, 15] and retrieval-augmented generation (RAG) [24]. However, when processing long sequences, LLM inference requires a significant amount of memory and is memory-bound [22, 19].

One of the major causes is the large size of key-value (KV) cache, which linearly increases with the sequence length. To alleviate this issue, many studies have proposed approaches to compressing KV cache effectively, such as eviction [44, 25, 4, 32] and low-rank approximation [5, 26]. Among them, quantization is one of the most widely adopted approaches. Previous studies [30, 19] analyze how outliers emerge in the KV cache and propose to quantize key and value along the channel dimension and token dimension, respectively. Recently, Coupled Quantization (CQ) [43] proposed to quantize multiple channels together, using centroids obtained from the calibration set. The idea of CQ is identical to the concept of vector quantization (VQ), where groups of values are jointly quantized into codebook indices. Utilizing the centroids as codebooks, CQ achieves state-of-the-art performance in diverse tasks, proving the effectiveness of VQ in KV cache quantization.

In our study, we observe that CQ fails to generalize in out-of-distribution (OOD) scenarios where the input distribution is different from that of the calibration set (in-distribution) [42]. For example, Figure 1a shows that while CQ excels in WikiText-2, it performs much worse in C4, since it is

*Corresponding author.

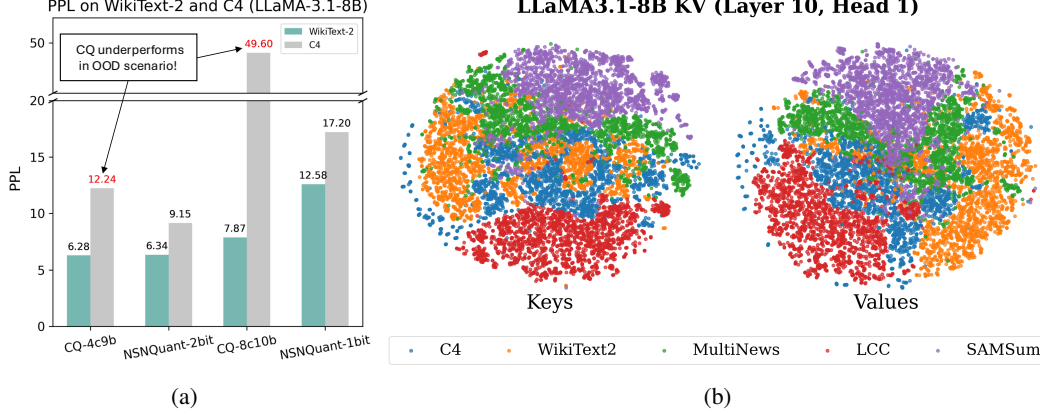


Figure 1: (a) PPL evaluation results with LLaMA3.1-8B. Although CQ achieves lower PPL in WikiText-2 (in-distribution), it performs worse on C4 (out-of-distribution). (b) t-SNE visualization of LLaMA3.1-8B key and value. The clustering pattern shows that key and value distributions strongly depend on the input data. More visualization can be found in Figure 11

calibrated using only a few samples from WikiText-2 dataset. Moreover, Figure 1b demonstrates the distribution of key and value can vary greatly by the input distribution. This implies that learning centroids from the small set of data is very risky when applying them to other datasets. To this end, we propose NSNQuant, a calibration-free vector quantization (VQ) method that generalizes well to a wide range of datasets. Our contributions are summarized as follows:

- We empirically show that the strong dependence of key-value distributions on the input dataset can lead to severe errors in the existing VQ method. In particular, we observe that the centroids learned by CQ-4c9b fail to accurately quantize important punctuation tokens in LLaMA3-8B and LLaMA3.1-8B on C4, resulting in degraded performance.
- To address this limitation, we propose **NSNQuant**, a calibration-free VQ method for KV cache. NSNQuant effectively matches the key and value distribution with the standard normal distribution through the Normalize-Shift-Normalize (NSN) process and the Hadamard transform, as shown in Figure 3. Since the approximate distribution of key-value is known prior to the inference, an effective codebook for VQ can be built without any external data.
- We conduct comprehensive experiments and analysis to show the effectiveness of NSNQuant across different tasks and models. The results with the LLaMA [31, 36, 14] and Mistral models [21] clearly show that NSNQuant outperforms other baselines in 1-bit and 2-bit quantization. Moreover, we implement efficient CUDA kernels for the low-bit computation, improving throughput and reducing memory usage.

2 Preliminary

LLM inference and KV cache LLM inference has two main stages: prefilling and decoding. In the prefilling stage, all prompt tokens are processed simultaneously by the transformer decoder layers [38]. In the decoding stage, new tokens are generated one by one in an autoregressive manner. In both stages, each token only attends to previous tokens due to the causal nature of masked self-attention. To avoid redundant computation, a KV cache stores key-value pairs from previous tokens. It is initialized during prefilling and updated at each decoding step by appending the latest key-value pair. It becomes a primary bottleneck when processing long sequences, as its size linearly increases with the sequence length.

Vector quantization Unlike scalar quantization (SQ) where each scalar value is quantized individually, vector quantization (VQ) compresses a group of values jointly using a codebook. In VQ, a d -dimensional vector is matched to the closest entry in a codebook, and quantized as follows:

$$\text{VQ}(v) = \underset{i}{\operatorname{argmin}} D(v, \mathbb{C}[i]), \quad (1)$$

where \mathbb{C} denotes the codebook and $D(a, b)$ is a distance function between vectors a and b .

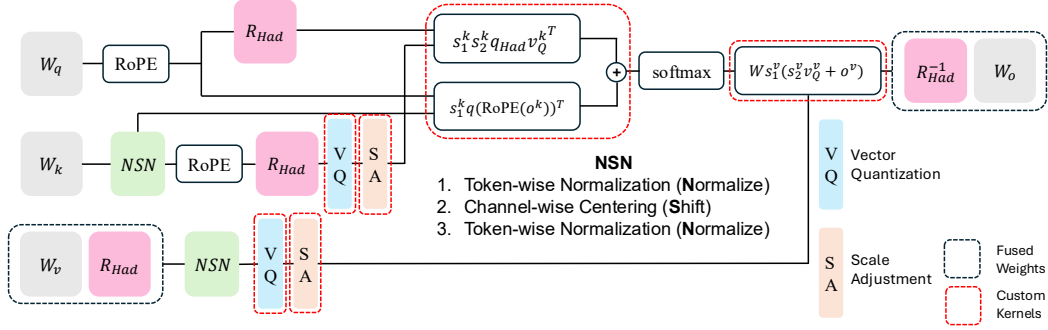


Figure 2: Overall structure of attention under NSNQuant. Residuals are omitted for simplicity. We use superscript k and v to mark values associated with key and value, respectively. Since NSN is applied to keys before RoPE, two branches are needed to correctly compute attention scores. See Appendix B for details on attention output computation.

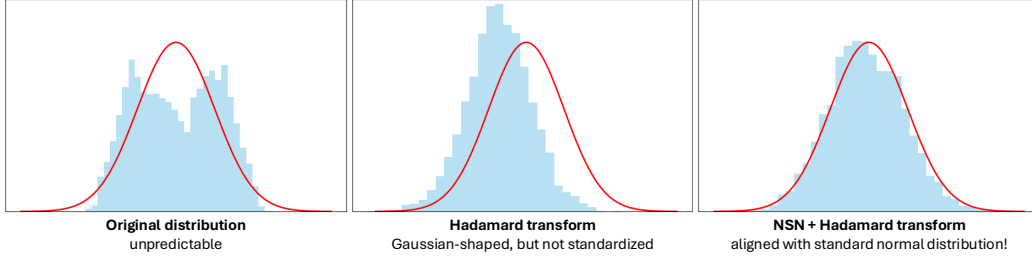


Figure 3: A visual illustration of the effect of NSN on the channel distribution. Our Normalize-Shift-Normalize (NSN) process aligns the channel distribution with the standard normal distribution, when used with the Hadamard transform.

Hadamard transform A Hadamard matrix is an orthogonal matrix whose entries all have the same magnitude. Its size can be doubled recursively through Sylvester’s construction, which builds a larger Hadamard matrix by combining copies of a smaller one in a specific pattern. This recursive definition forms the basis of the Walsh–Hadamard transform, allowing matrix–vector multiplication in $O(d \log d)$ time. QuIP# [37] adopts the **randomized Hadamard transform (RHT)** [16], where the sign of each row and column is flipped independently with probability 1/2. We also employ RHT to compute the theoretical bounds presented in Lemma 1.

3 Method

3.1 Motivation

As shown in Figure 1a, we observe several cases where the existing VQ method, coupled quantization (CQ) [43], suffers from severe performance degradation when tested on OOD datasets. We attribute this to the distribution mismatch between datasets, as visualized in Figure 1b. We observe that this mismatch can cause severe errors in certain datasets. A notable example of such errors is the large quantization error observed in punctuation tokens in LLaMA3-8B and LLaMA3.1-8B.

WikiText-2, a calibration dataset for CQ, only contains " , " (with whitespace) tokens, while the C4 dataset includes " ," (without whitespace) tokens. This mismatch leads to large errors for the keys corresponding to the punctuation token " ," in the first layer of LLaMA3 models, since the centroids of CQ are obtained only from WikiText-2. This leads to significant distortion in attention weights because in certain heads, the " ," token accounts for over 90% of the attention weights. By preserving the keys corresponding to these tokens in the first layer, the perplexity of CQ-4c9b on C4 is improved from 13.97 to 9.15 in LLaMA3-8B, and from 12.24 to 9.16 in LLaMA3.1-8B, closely matching the results of NSNQuant.

Table 1: Average channel-wise KL divergence with the standard normal distribution measured on key and value of LLaMA2-7B on WikiText-2 with sequence length of 4096. KL divergence is computed between the binned empirical distribution and the standard normal CDF. We used 4096 random data for Oracle, to match the sequence length.

Method	Key		Value	
	w/ Had.	w/o Had.	w/ Had.	w/o Had.
N	0.2476	0.5405	0.0817	0.1109
NS	0.3068	0.5261	0.0356	0.0666
NSN	0.0197	0.2230	0.0252	0.0537
Oracle (torch.randn)	0.0096			

To avoid these calibration-induced errors, we propose a calibration-free vector quantization (VQ) method, **NSNQuant**, which does not rely on any external data. While CQ tries to match the codebook to the key-value (KV) distribution, we instead propose to match the KV distribution to a well-known prior. Motivated by the recent success of Hadamard-based methods in producing normal-like output distributions regardless of the input, we introduce a novel transformation—*Normalize-Shift-Normalize* (NSN)—that aligns key and value channels to a standard normal distribution. This enables us to construct a single reusable codebook tailored for the standard normal distribution, making our method, NSNQuant, both calibration-free and robust across diverse inputs.

The overall structure of NSNQuant is depicted in Figure 2. Key-value tokens are first processed through the NSN and Hadamard transform. They are then compressed by vector quantization (VQ) using a codebook, and a scaling parameter s_2 is adjusted adaptively to the VQ result. The detailed process of NSN is described in Section 3.2. The post-scaling technique and the recipe for building a codebook are introduced in Section 3.3 and 3.4, respectively.

3.2 Normalize-Shift-Normalize (NSN)

NSN consists of three steps: **1**) a token-wise normalization (*Normalize*), **2**) a channel-wise centering (*Shift*), **3**) a second token-wise normalization (*Normalize*).

Let $v \in \mathbb{R}^{l \times d}$ be the tensor where l is a sequence length and d is a hidden dimension per head. In the first *Normalize* step, each token is normalized to have a norm of \sqrt{d} , where d is a token dimension per head. This prevents outlier tokens [7] from dominating the next steps and incurring large errors in tokens with small magnitude. In the *Shift* step, channel-wise mean is calculated and subtracted, so that the resulting distribution is zero-centered. Finally, in the second *Normalization* step, each token is again normalized to have a norm \sqrt{d} . The entire process is formulated as follows:

1. **Normalize:** $s_1 \leftarrow \text{norm}(v, \text{dim}=\text{token})/\sqrt{d}$, $v_n \leftarrow v/s_1$
2. **Shift:** $o \leftarrow \text{mean}(v_n, \text{dim}=\text{channel})$, $v_{ns} \leftarrow v_n - o$
3. **Normalize:** $s_2 \leftarrow \text{norm}(v_{ns}, \text{dim}=\text{token})/\sqrt{d}$, $v_{nsn} \leftarrow v_{ns}/s_2$

Each step produces a byproduct—denoted as s_1 , o , and s_2 —which is used to restore the original tensor by $v = s_1(s_2 v_{nsn} + o)$. Although the last step can deviate the channel-wise mean from zero, we find that its effect is negligible, as further discussed in Appendix D.1.

When used together with the subsequent Hadamard transform, our NSN process effectively aligns the channel distribution with the standard normal distribution. ① As identified in previous studies [37, 39, 9, 20], the Hadamard transform results in a normal-like distribution, which is supported by the central limit theorem. ② NSN process roughly standardizes the distribution of each channel when used with the following Hadamard transform. Putting ① and ② together, the resulting channel distribution is aligned with the standard normal distribution. ② can be justified through the following lemma, which gives theoretical bounds for variances:

Lemma 1. Let $X = (X_1, \dots, X_d)^\top \in \mathbb{R}^d$ be the random vector from the joint distribution of the channels after the NSN process, which satisfies

$$(1) \text{ Nearly centered: } \frac{1}{d} \sum_{i=1}^d (\mathbb{E}[X_i])^2 \leq \varepsilon, \quad (2) \text{ Normalized: } \sum_{i=1}^d \mathbb{E}[X_i^2] = d,$$

(3) Covariance bound: $\|\text{Cov}(X) - \text{diag}(\text{Cov}(X))\|_F \leq \Gamma$.

For the randomized Hadamard transform $Y = \text{RHT}(X)$, $0 < \alpha < 1$ and $i \in \{1, 2, \dots, d\}$,

$$\mathbb{P}\left(\text{Var}(Y_i) \in [1 - \varepsilon - \Gamma \beta_\alpha, 1 + \Gamma \beta_\alpha]\right) \geq 1 - \alpha$$

where $\beta_\alpha := \frac{1}{d} \sqrt{\frac{\ln(2/\alpha)}{c}}$ and c is a constant from the Hanson-Wright inequality [34].

The proof for the lemma is provided in Appendix A.1. Here, we adopt randomized Hadamard transform (RHT) to make the probabilistic claim, but using the naive Hadamard transform works well in practice, as presented in Table 6. Since NSN tightens the bound ε , and Γ is small for most of the layers, we observe that the resulting variances are generally close to 1. However, we find that it does not hold in certain heads in the early layers, as presented in Figures 12 and 13. This is due to the presence of outlier channels with huge variances in the first layer, which enlarges the bound Γ . Despite this limitation, Figure 5 demonstrates that the quantization error remains low in these layers as well. We leave it to future work to explicitly model and account for these exceptions.

Residual To implement the second step (Shift) in the decoding stage, we bring the idea of *residual* from KIVI [30]. Following KIVI, we split KV cache into two parts: one part with quantized KV cache, and the other part with full-precision KV cache (residual). If the size of the residual reaches its maximum capacity, the KV cache in the residual is flushed, quantized, and appended to the quantized part. We introduce a hyperparameter called *residual size* to control the size of the residual. To ensure consistency, we also apply NSN in residual-size chunks during the prefilling stage. In our experiments, we set the residual size to 64.

NSN applied to key and value As illustrated in Figure 2, NSN is applied slightly differently to the key and value. For keys, NSN is applied immediately after the projection layer, and v_{nsn} is quantized following the RoPE and Hadamard transform. While applying NSN after RoPE may seem more straightforward since RoPE might affect the channel-wise mean, we find that this ordering yields better quantization quality. Since RoPE is not applied to o yet, we instead apply it within our custom kernel when computing attention scores, as shown in the figure. For values, the Hadamard transform is fused into the projection layers, and NSN is applied right afterward. Note that since the Hadamard transform is equivalent to multiplication by a rotation matrix, its order with the adjacent NSN does not change the output.

3.3 Scale adjustment

Let $v \in \mathbb{R}^d$ be a token vector which is processed by the NSN and Hadamard transform. It is then divided into 8-dimensional sub-vectors and quantized using the codebook, following the objective in Equation 1. Let v_Q be the vector restored by looking up codebook. i.e., $v_Q = \mathbb{C}[\text{VQ}(v)]$. We find that rather than using v_Q as-is, scaling v_Q adaptively improves performance. Specifically, we find that it is beneficial to scale v_Q as follows, which is identical to scaling s_2 since v_Q is multiplied by s_2 when restoring:

$$v_Q \leftarrow \frac{\|v\|_2^2}{v \cdot v_Q} v_Q \quad (\text{i.e., } s_2 \leftarrow \frac{\|v\|_2^2}{v \cdot v_Q} s_2).$$

This is a scaling strategy which makes $v_Q - v$ orthogonal to v . In other words, it preserves components parallel to v , while allowing some orthogonal errors. Interpreting o as local context and v as a distinctive token feature, this strategy can be interpreted as making each token distinctive, which is essential for KV cache considering its selective property. We provide comparison for different scaling strategies in Appendix C.3.

3.4 Codebook tuning

We construct a single global codebook for compressing 8-dimensional vectors using integer indices, following QuIP# [37]. NSNQuant-2b uses 8 bits for signs and 8 for codebook indices, while NSNQuant-1b uses only 8 bits for indices. A simple baseline can be built via K-Means on standard normal data, but its local optimality limits performance. We improve this by fine-tuning on synthetic

standard normal data (`torch.randn`) to minimize cosine distance between original and quantized vectors, since the error of scale adjustment depends only on the angle between them. As the lookup is non-differentiable, gradients are propagated only through post-lookup operations. The PyTorch implementation for this process runs less than 5 minutes on an RTX 3090, unlike calibration process of CQ or KVQuant which requires backpropagation through model weights. While E8P [37] is also a competitive 2-bit baseline, it is hard to apply to the 1-bit scenario, and requires expensive comparisons with over 2000 entries. We provide comparison results in Table 9.

3.5 Double quantization

To further reduce the memory overhead, we employ double quantization (DQ) proposed in QLoRA [10], which quantizes parameters used for the quantization. Specifically, we quantize o and s_1 with a group size of 32 and *residual size*, respectively, using 4-bit round-to-nearest (RTN) quantization. DQ significantly reduces the average bit width. As a result, NSNQuant costs only additional 0.23 bits on average for the NSN process, when residual size is set to 64. Moreover, to reduce the amount of shared memory required for the codebook, we also apply 4-bit quantization to codebook entries. As shown in Table 11, DQ barely affects the effectiveness of NSNQuant.

3.6 Efficient kernel implementation

We implement the CUDA kernels for efficient execution of NSNQuant-2b and NSNQuant-1b. For codebook matching, we compute and manage distances on-the-fly in streaming multiprocessors (SMs), while loading codebook tiles into shared memory. For dequantization and matrix-vector multiplications, our kernel loads the codebook into shared memory to minimize the accesses to DRAM. We implement two different kernels for QK^T and WV (W : attention weights) since they use different axis for reduction. We also fuse the computation of both the quantized and the residual parts to maximize GPU utilization even in the small-batch scenarios.

4 Experiments

4.1 Experimental setup

Datasets First, we evaluate perplexity (PPL) on WikiText-2 and C4 dataset to show quantization error in language modeling. Second, we report evaluation results on LongBench [3]. We choose the task subset from LongBench following KIVI [30]: Qasper for a single-document QA task; QMSum and MultiNews for summarization tasks; TREC, TriviaQA and SAMSum for few-shot learning tasks; LCC and RepoBench-P for code completion tasks. Lastly, we run evaluations on GSM8K [8], HumanEval [6], CoQA [33], and MMLU [18] using LM-Eval framework [13] to test generation capability in more diverse generation scenarios.

Baselines We compare NSNQuant against four baselines: KIVI [30], KIVI + Hadamard, KVQuant [19], and CQ [43]. While some of these methods provide multiple versions with similar average bits (e.g., CQ-4c8b and CQ-4c9b), we adopt the stronger variants to better demonstrate the superiority of our approach. Simpler baselines like INT2 are excluded, as prior studies [19, 43] have shown them to be ineffective. For NSNQuant, we fix both residual size to 64. For KIVI, we use a group size of 64 for keys and 128 for tokens, to maintain consistency with our residual policy. Detailed explanations for each baseline are provided in Appendix E.3. Note that since CQ does not provide their official implementation, we reproduce it based on the official implementation of KVQuant. The result of CQ is slightly worse than the one reported in the original paper.

Policy for full-precision cache Since maintaining full-precision cache largely affects generation quality [30, 43], we unify several settings to focus only on quantization quality: all methods adopt NSNQuant’s residual policy, which buffers full-precision caches until the residual is full. We fix the residual size to 64 in all experiments. Attention sink-aware quantization is removed from KVQuant, as it can be easily applied to other methods as well. Since some methods (e.g., KIVI) use full-precision cache in the prefilling stage, while others (e.g., CQ) use quantized cache, we standardize this by using full-precision cache in the prefilling stage for all methods—except in perplexity evaluations, where key and value quantization is necessary to measure forward-pass quality.

4.2 PPL evaluation

Table 2: Perplexity on WikiText-2 and C4 with a context length of 4096. The results of CQ reported in the original paper are marked with †.

Method	Avg. bit width	Dataset	LLaMA2-7B	LLaMA2-13B	LLaMA3-8B	LLaMA3.1-8B	Mistral-7B-v0.3
FP16	16	C4	6.63	6.04	8.32	8.43	7.48
		WikiText-2	5.12	4.57	5.75	5.84	4.95
KIVI-2	2.38	C4	8.00	7.03	16.43	15.80	8.83
		WikiText-2	6.14	5.30	10.93	10.55	6.03
KIVI-2 + Had	2.38	C4	7.57	6.68	12.67	12.54	8.43
		WikiText-2	5.79	5.05	8.69	8.86	5.65
KVQuant-2b + 1%	2.32	C4	7.09	6.37	<u>9.75</u>	<u>9.60</u>	7.93
		WikiText-2	5.52	4.88	6.74	6.71	5.32
CQ-4c9b	2.26	C4	7.12 (<u>7.02†</u>)	6.45 (<u>6.36†</u>)	13.97	12.24	<u>7.86</u>
		WikiText-2	5.36 (<u>5.32†</u>)	4.76 (<u>4.74†</u>)	6.16	6.28	<u>5.16</u>
NSNQuant-2b	2.23	C4	6.86	6.21	9.08	9.15	7.69
		WikiText-2	5.29	4.71	<u>6.23</u>	<u>6.34</u>	5.12
KVQuant-1b + 1%	1.32	C4	30.79	14.27	<u>33.17</u>	<u>37.37</u>	12.45
		WikiText-2	13.5	9.91	27.57	33.96	9.06
CQ-8c10b	1.27	C4	9.25 (<u>9.12†</u>)	8.17 (<u>8.01†</u>)	43.78	49.60	9.60
		WikiText-2	6.33 (6.25†)	5.53 (5.47†)	7.69	7.87	6.01
NSNQuant-1b	1.23	C4	8.70	7.55	16.69	17.20	<u>9.67</u>
		WikiText-2	<u>6.69</u>	<u>5.70</u>	<u>11.70</u>	<u>12.58</u>	<u>6.66</u>

Table 2 presents the perplexity (PPL) of various models evaluated on WikiText2 and C4. Although our framework uses full-precision key and value during the prefilling stage, we follow the evaluation protocol of CQ and KVQuant by quantizing them all in this experiment. Despite its difference from the generation scenario, we find PPL evaluation useful because it measures quantization quality for a sequence with a single forward pass. Furthermore, the results are aligned with those in Table 15, where we report the PPL evaluation results in the generation scenario with residuals. Therefore, we report PPL results in the main table, and use them in ablation studies.

Across both datasets, CQ and NSNQuant outperform the other methods. On WikiText-2, the two methods exhibit comparable performance in 2-bit quantization, with CQ outperforming NSNQuant in the 1-bit setting. However, on C4, NSNQuant consistently outperforms CQ in both 2-bit and 1-bit quantization. Notably, CQ suffers from severe performance degradation on C4 when using LLaMA3-8B and LLaMA3.1-8B, whereas NSNQuant maintains strong performance. These results suggest that NSNQuant generalizes better across datasets, while CQ struggles under distribution shift from the calibration dataset.

4.3 LongBench evaluation

Table 3: Evaluation results on LongBench. The task subset is selected following KIVI [30]. More results with different models can be found in Table 16.

Model	Method	Bits	Qasper	QMSum	MultiNews	TREC	TriviaQA	SAMSum	LCC	RepoBench-P	Avg.
LLaMA3.1-8B-Instruct	FP16	16	13.11	23.53	26.74	72.50	91.65	43.78	63.04	56.17	48.82
	KIVI-2	2.38	12.04	24.96	26.70	72.00	91.97	43.43	60.85	53.39	48.17
	KIVI-2 + Had	2.38	11.57	24.28	26.51	72.50	92.09	43.21	62.90	55.20	<u>48.53</u>
	KVQuant-2b + 1%	2.32	13.15	23.45	26.24	72.00	91.63	41.39	60.80	54.41	47.88
	CQ-4c9b	2.26	12.25	23.80	25.74	71.50	91.53	41.96	61.18	54.46	47.80
	NSNQuant-2b	2.23	12.44	23.74	26.95	72.50	91.73	44.01	62.05	55.09	48.56
	KVQuant-1b + 1%	1.32	9.91	22.19	22.27	47.50	88.92	35.76	50.27	43.79	40.08
	CQ-8cb10	1.27	8.84	21.18	22.40	47.50	87.94	38.86	53.81	45.73	<u>40.78</u>
	NSNQuant-1b	1.23	11.54	24.69	27.16	71.50	92.04	42.36	60.08	49.70	47.38
Mistral-7B-Instruct-v0.3	FP16	16	41.13	25.75	27.78	76.00	88.59	47.47	59.52	60.64	53.36
	KIVI-2	2.38	37.86	24.62	26.85	76.00	88.51	45.93	58.72	57.87	52.05
	KIVI-2 + Had	2.38	39.99	25.42	27.50	76.00	88.42	46.52	59.54	60.13	52.94
	KVQuant-2b + 1%	2.32	38.98	25.10	27.22	76.00	89.02	45.27	58.57	61.59	52.72
	CQ-4c9b	2.26	39.85	24.50	27.19	76.00	88.86	45.56	58.36	60.26	52.57
	NSNQuant-2b	2.23	39.96	24.91	27.54	76.00	88.96	46.47	58.70	59.45	<u>52.75</u>
	KVQuant-1b + 1%	1.32	28.58	21.89	22.76	50.50	87.75	39.62	54.73	54.46	45.04
	CQ-8c10b	1.27	31.21	22.56	23.12	64.50	88.09	41.71	53.82	52.31	<u>47.16</u>
	NSNQuant-1b	1.23	37.94	25.03	26.81	76.00	89.39	46.37	56.75	55.57	51.73

Table 3 gives performance comparison on LongBench. In 1-bit quantization, NSNQuant-1b outperforms other baselines by a large margin. However, in 2-bit quantization, all methods exhibit similar performances. We attribute this trend to the noisy nature of certain tasks. For example, in code generation tasks like LCC and RepoBench-P, models tend to generate additional descriptions of the codes. These descriptions do not hurt the code quality, but eventually degrade the metric. To this end, for tasks with potentially noisy metrics, we also report the ROUGE-L score with the FP16 output to measure how well each method preserves the original model output. Table 17 clearly shows that NSNQuant best preserves the original model outputs.

4.4 Evaluation on more datasets

Table 4: Evaluation results on GSM8K, HumanEval, CoQA, and MMLU. Accuracy is reported for all tasks. Results with LLaMA2-13B-Chat and LLaMA3-8B-Instruct can be found in Table 18

Model	Method	Bits	GSM8K (8-shot, CoT)	HumanEval	CoQA	MMLU (4-shot, CoT)			
						Humanities	STEM	Social	Other
LLaMA3.1-8B-Instruct	FP16	16	76.65	57.93	63.78	71.47	57.96	74.16	72.52
	KIVI-2	2.38	64.59	48.17	63.60	64.44	50.09	66.84	66.13
	KIVI-2 + Had	2.38	65.73	50.61	63.88	67.73	53.03	68.50	68.14
	KVQuant-2b + 1%	2.32	70.05	<u>53.05</u>	62.37	68.18	54.78	71.31	69.61
	CQ-4c9b	2.26	72.93	48.78	62.93	67.07	52.66	70.22	69.33
	NSNQuant-2b	2.23	75.89	56.10	<u>63.83</u>	71.04	55.64	73.42	70.74
	KVQuant-1b + 1%	1.32	21.53	23.17	53.55	23.04	11.23	37.59	33.02
	CQ-8c10b	1.27	<u>44.88</u>	<u>25.61</u>	<u>56.58</u>	<u>28.21</u>	<u>21.34</u>	<u>31.97</u>	<u>41.10</u>
	NSNQuant-1b	1.23	53.45	44.51	62.70	59.82	45.83	65.34	63.77
	FP16	16	53.15	31.10	65.58	65.98	50.46	71.06	68.26
Mistral-7B-Instruct-v0.3	KIVI-2	2.38	43.75	28.66	64.45	60.96	39.93	63.52	59.05
	KIVI-2 + Had	2.38	46.10	28.05	<u>65.48</u>	<u>63.28</u>	45.11	66.99	63.07
	KVQuant-2b + 1%	2.32	46.63	27.44	64.28	63.00	<u>45.47</u>	67.39	<u>66.27</u>
	CQ-4c9b	2.26	<u>47.84</u>	31.10	64.80	62.48	42.48	<u>68.73</u>	63.98
	NSNQuant-2b	2.23	51.02	31.10	65.62	64.92	47.65	69.11	67.56
	KVQuant-1b + 1%	1.32	16.30	19.51	55.95	16.48	9.88	17.18	14.21
	CQ-8c10b	1.27	<u>25.93</u>	<u>21.95</u>	<u>59.07</u>	<u>23.77</u>	<u>17.62</u>	<u>27.09</u>	<u>19.78</u>
	NSNQuant-1b	1.23	38.89	27.44	63.60	58.52	40.34	62.34	58.43
	FP16	16	53.15	31.10	65.58	65.98	50.46	71.06	68.26
	KIVI-2	2.38	43.75	28.66	64.45	60.96	39.93	63.52	59.05

In addition to the LongBench results, we further evaluate the models on GSM8K (mathematical reasoning), HumanEval (code generation), CoQA (conversational question answering), and MMLU (multi-task language understanding) to provide a more comprehensive assessment of generation quality. As shown in Table 4, NSNQuant outperforms other baselines in most of the settings. In particular, NSNQuant excels in GSM8K and MMLU in a few-shot CoT (Chain-of-Thought) setting, which requires models to generate an exact and strict reasoning path.

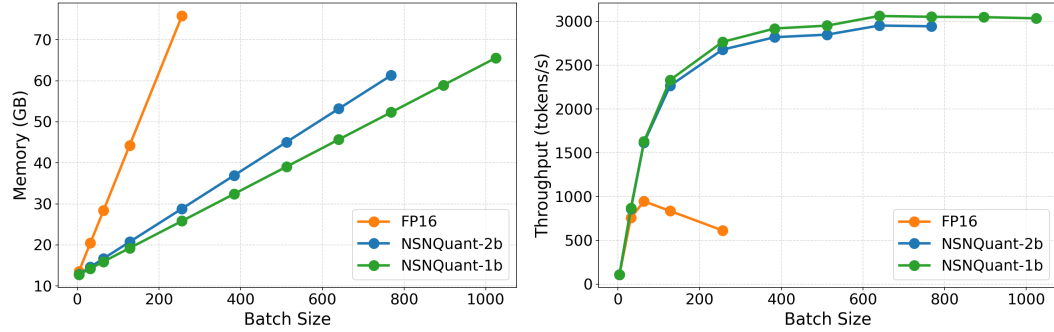


Figure 4: Peak memory usage (left) and throughput (right) measured with varying batch sizes. The residual size is set to 64. Results with varying residual sizes are available in Figure 8.

4.5 Efficiency analysis

To evaluate time and memory efficiency of NSNQuant, we measure memory usage and throughput of NSNQuant. Following previous works [30, 23], we use the synthetic data to simulate the scenario of ShareGPT [35] where the average input length is 161 and the average generation length is 338. The evaluation is performed on a linux server with a single A100-80GB GPU with LLaMA2-7B.

The result is illustrated in Figure 4. While FP16 baseline suffers from OOM for large batch sizes, NSNQuant-2b and NSNQuant-1b scale efficiently to larger batch sizes, achieving 4× larger batch

Table 5: PPL measured on WikiText-2 with LLaMA2-7B without each component of NSNQuant-2b.

Method	PPL
NSNQuant-2b	5.285
w/o first token-wise normalization	6.293
w/o channel-wise centering	5.842
w/o second token-wise normalization	5.456
w/o Hadamard transform	5.730

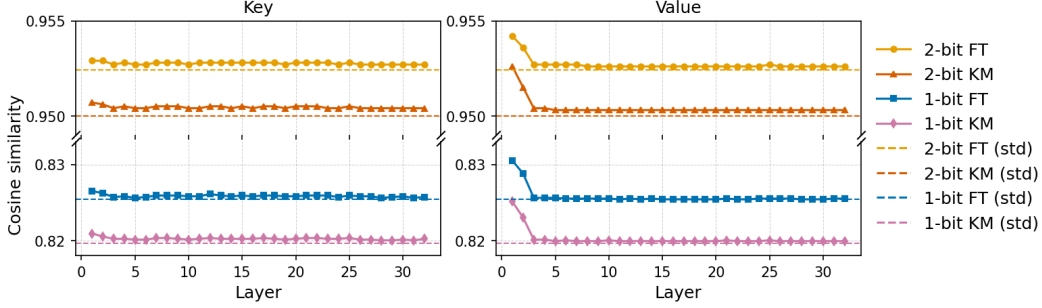


Figure 5: Cosine similarity between original and reconstructed vectors when applying VQ to the NSN-processed keys and values of LLaMA2-7B. Similarities are measured on WikiText-2 dataset with different codebooks. KM denotes the K-Means codebook, and FT denotes the fine-tuned codebook. The lines with markers show cosine similarity measured using the key-value from the model, whereas the dotted lines show measurements using synthetic standard normal data.

sizes and $3\times$ speedup in throughput. Note that the memory increases are not proportional to average bits since the residual is also included in the memory usage.

4.6 Ablation study

Effects of the NSN and Hadamard To assess the contribution of each NSN component and the Hadamard transform, we measure perplexity on WikiText-2 while removing them individually. As shown in Table 5, skipping any step results in higher perplexity. This trend aligns with Table 1, which shows using NSN and the Hadamard transform together leads to the best alignment. The first token-wise normalization has the greatest impact, as it suppresses outlier tokens before centering. In contrast, the second token-wise normalization has minimal effect, suggesting that channel-wise centering does not significantly alter token scale.

Effects of codebook tuning The Figure 5 shows the cosine similarity between the original vector v and the quantized vector $v_Q := \mathbb{C}[\text{VQ}(v)]$ with different codebooks. The fine-tuned version gives higher cosine similarities compared to the K-Means codebook. Furthermore, the cosine similarities are consistently high in the early layers, although the standardization of NSN does not hold in these layers. Notably, the cosine similarities measured using the key-value tokens (lines with markers) are very similar to those measured using synthetic standard normal data (dotted lines). This suggests that NSN successfully aligns the output distribution with the standard normal distribution, and the codebook trained only on synthetic data effectively quantizes such outcomes. As a result, codebook tuning improves perplexity from 5.294 to 5.285 with NSNQuant-2b and 6.910 to 6.703 with NSNQuant-1b.

5 Conclusion

In this work, we propose NSNQuant, a calibration-free vector quantization (VQ) method for compressing KV cache of LLMs. NSNQuant effectively aligns the token distribution with the standard normal distribution through the NSN (Normalize-Shift-Normalize) process, enabling the use of the specialized codebook for the standard normal distribution. Through extensive experiments, we demonstrate that unlike calibration-based VQ methods, NSNQuant generalizes well across different tasks and datasets. In particular, NSNQuant excels in 1-bit quantization, outperforming the previous state-of-the-art method by a huge gap. We also implement efficient CUDA kernels for NSNQuant, and verify that NSNQuant achieves a $3\times$ speedup compared to the FP16 baseline.

Acknowledgements

We are grateful to VESSL AI for providing the compute resources used for the experiments in this work.

References

- [1] Josh Achiam, Steven Adler, Sandhini Agarwal, Lama Ahmad, Ilge Akkaya, Florencia Leoni Aleman, Diogo Almeida, Janko Altschmidt, Sam Altman, Shyamal Anadkat, et al. Gpt-4 technical report. *arXiv preprint arXiv:2303.08774*, 2023.
- [2] Saleh Ashkboos, Amirkeivan Mohtashami, Maximilian Croci, Bo Li, Pashmina Cameron, Martin Jaggi, Dan Alistarh, Torsten Hoefer, and James Hensman. Quarot: Outlier-free 4-bit inference in rotated llms. *Advances in Neural Information Processing Systems*, 37:100213–100240, 2025.
- [3] Yushi Bai, Xin Lv, Jiajie Zhang, Hongchang Lyu, Jiankai Tang, Zhidian Huang, Zhengxiao Du, Xiao Liu, Aohan Zeng, Lei Hou, Yuxiao Dong, Jie Tang, and Juanzi Li. LongBench: A bilingual, multitask benchmark for long context understanding. In Lun-Wei Ku, Andre Martins, and Vivek Srikumar, editors, *Proceedings of the 62nd Annual Meeting of the Association for Computational Linguistics (Volume 1: Long Papers)*, pages 3119–3137, Bangkok, Thailand, August 2024. Association for Computational Linguistics.
- [4] Zefan Cai, Yichi Zhang, Bofei Gao, Yuliang Liu, Tianyu Liu, Keming Lu, Wayne Xiong, Yue Dong, Baobao Chang, Junjie Hu, et al. Pyramidkv: Dynamic kv cache compression based on pyramidal information funneling. *arXiv preprint arXiv:2406.02069*, 2024.
- [5] Chi-Chih Chang, Wei-Cheng Lin, Chien-Yu Lin, Chong-Yan Chen, Yu-Fang Hu, Pei-Shuo Wang, Ning-Chi Huang, Luis Ceze, Mohamed S Abdelfattah, and Kai-Chiang Wu. Palu: Kv-cache compression with low-rank projection. In *The Thirteenth International Conference on Learning Representations*.
- [6] Mark Chen, Jerry Tworek, Heewoo Jun, Qiming Yuan, Henrique Ponde de Oliveira Pinto, Jared Kaplan, Harri Edwards, Yuri Burda, Nicholas Joseph, Greg Brockman, Alex Ray, Raul Puri, Gretchen Krueger, Michael Petrov, Heidy Khlaaf, Girish Sastry, Pamela Mishkin, Brooke Chan, Scott Gray, Nick Ryder, Mikhail Pavlov, Alethea Power, Lukasz Kaiser, Mohammad Bavarian, Clemens Winter, Philippe Tillet, Felipe Petroski Such, Dave Cummings, Matthias Plappert, Fotios Chantzis, Elizabeth Barnes, Ariel Herbert-Voss, William Hebggen Guss, Alex Nichol, Alex Paino, Nikolas Tezak, Jie Tang, Igor Babuschkin, Suchir Balaji, Shantanu Jain, William Saunders, Christopher Hesse, Andrew N. Carr, Jan Leike, Josh Achiam, Vedant Misra, Evan Morikawa, Alec Radford, Matthew Knight, Miles Brundage, Mira Murati, Katie Mayer, Peter Welinder, Bob McGrew, Dario Amodei, Sam McCandlish, Ilya Sutskever, and Wojciech Zaremba. Evaluating large language models trained on code. 2021.
- [7] Mengzhao Chen, Yi Liu, Jiahao Wang, Yi Bin, Wenqi Shao, and Ping Luo. Prefixquant: Static quantization beats dynamic through prefixed outliers in llms. *arXiv preprint arXiv:2410.05265*, 2024.
- [8] Karl Cobbe, Vineet Kosaraju, Mohammad Bavarian, Mark Chen, Heewoo Jun, Lukasz Kaiser, Matthias Plappert, Jerry Tworek, Jacob Hilton, Reiichiro Nakano, et al. Training verifiers to solve math word problems. *arXiv preprint arXiv:2110.14168*, 2021.
- [9] Nachshon Cohen, Amit Portnoy, Besnik Fetahu, and Amir Ingber. Sdr: Efficient neural re-ranking using succinct document representation. *arXiv preprint arXiv:2110.02065*, 2021.
- [10] Tim Dettmers, Artidoro Pagnoni, Ari Holtzman, and Luke Zettlemoyer. Qlora: Efficient finetuning of quantized llms, 2023. URL <https://arxiv.org/abs/2305.14314>, 2, 2023.
- [11] Vage Egiazarian, Andrei Panferov, Denis Kuznedelev, Elias Frantar, Artem Babenko, and Dan Alistarh. Extreme compression of large language models via additive quantization. *arXiv preprint arXiv:2401.06118*, 2024.

- [12] Elias Frantar, Saleh Ashkboos, Torsten Hoefler, and Dan Alistarh. Gptq: Accurate post-training quantization for generative pre-trained transformers. *arXiv preprint arXiv:2210.17323*, 2022.
- [13] Leo Gao, Jonathan Tow, Baber Abbasi, Stella Biderman, Sid Black, Anthony DiPofi, Charles Foster, Laurence Golding, Jeffrey Hsu, Alain Le Noac’h, Haonan Li, Kyle McDonell, Niklas Muennighoff, Chris Ociepa, Jason Phang, Laria Reynolds, Hailey Schoelkopf, Aviya Skowron, Lintang Sutawika, Eric Tang, Anish Thite, Ben Wang, Kevin Wang, and Andy Zou. A framework for few-shot language model evaluation, 07 2024.
- [14] Aaron Grattafiori, Abhimanyu Dubey, Abhinav Jauhri, Abhinav Pandey, Abhishek Kadian, Ahmad Al-Dahle, Aiesha Letman, Akhil Mathur, Alan Schelten, Alex Vaughan, et al. The llama 3 herd of models. *arXiv preprint arXiv:2407.21783*, 2024.
- [15] Daya Guo, Dejian Yang, Haowei Zhang, Junxiao Song, Ruoyu Zhang, Runxin Xu, Qihao Zhu, Shirong Ma, Peiyi Wang, Xiao Bi, et al. Deepseek-r1: Incentivizing reasoning capability in llms via reinforcement learning. *arXiv preprint arXiv:2501.12948*, 2025.
- [16] Nathan Halko, Per-Gunnar Martinsson, and Joel A Tropp. Finding structure with randomness: Probabilistic algorithms for constructing approximate matrix decompositions. *SIAM review*, 53(2):217–288, 2011.
- [17] Yefei He, Luoming Zhang, Weijia Wu, Jing Liu, Hong Zhou, and Bohan Zhuang. Zipcache: Accurate and efficient kv cache quantization with salient token identification. *arXiv preprint arXiv:2405.14256*, 2024.
- [18] Dan Hendrycks, Collin Burns, Steven Basart, Andy Zou, Mantas Mazeika, Dawn Song, and Jacob Steinhardt. Measuring massive multitask language understanding. *arXiv preprint arXiv:2009.03300*, 2020.
- [19] Coleman Hooper, Sehoon Kim, Hiva Mohammadzadeh, Michael W Mahoney, Sophia Shao, Kurt Keutzer, and Amir Gholami. Kvquant: Towards 10 million context length llm inference with kv cache quantization. *Advances in Neural Information Processing Systems*, 37:1270–1303, 2024.
- [20] Xing Hu, Yuan Cheng, Dawei Yang, Zukang Xu, Zhihang Yuan, Jiangyong Yu, Chen Xu, Zhe Jiang, and Sifan Zhou. Ostquant: Refining large language model quantization with orthogonal and scaling transformations for better distribution fitting. *arXiv preprint arXiv:2501.13987*, 2025.
- [21] Albert Q. Jiang, Alexandre Sablayrolles, Arthur Mensch, Chris Bamford, Devendra Singh Chaplot, Diego de las Casas, Florian Bressand, Gianna Lengyel, Guillaume Lample, Lucile Saulnier, L  lio Renard Lavaud, Marie-Anne Lachaux, Pierre Stock, Teven Le Scao, Thibaut Lavril, Thomas Wang, Timoth  e Lacroix, and William El Sayed. Mistral 7b, 2023.
- [22] Sehoon Kim, Coleman Hooper, Amir Gholami, Zhen Dong, Xiuyu Li, Sheng Shen, Michael W Mahoney, and Kurt Keutzer. Squeezellm: Dense-and-sparse quantization. *arXiv preprint arXiv:2306.07629*, 2023.
- [23] Woosuk Kwon, Zhuohan Li, Siyuan Zhuang, Ying Sheng, Lianmin Zheng, Cody Hao Yu, Joseph Gonzalez, Hao Zhang, and Ion Stoica. Efficient memory management for large language model serving with pagedattention. In *Proceedings of the 29th Symposium on Operating Systems Principles*, pages 611–626, 2023.
- [24] Patrick Lewis, Ethan Perez, Aleksandra Piktus, Fabio Petroni, Vladimir Karpukhin, Naman Goyal, Heinrich K  ttler, Mike Lewis, Wen-tau Yih, Tim Rockt  schel, et al. Retrieval-augmented generation for knowledge-intensive nlp tasks. *Advances in neural information processing systems*, 33:9459–9474, 2020.
- [25] Yuhong Li, Yingbing Huang, Bowen Yang, Bharat Venkitesh, Acyr Locatelli, Hanchen Ye, Tianle Cai, Patrick Lewis, and Deming Chen. Snapkv: Llm knows what you are looking for before generation. *Advances in Neural Information Processing Systems*, 37:22947–22970, 2024.

- [26] Bokai Lin, Zihao Zeng, Zipeng Xiao, Siqi Kou, Tianqi Hou, Xiaofeng Gao, Hao Zhang, and Zhijie Deng. Matryoshkakv: Adaptive kv compression via trainable orthogonal projection. *arXiv preprint arXiv:2410.14731*, 2024.
- [27] Ji Lin, Jiaming Tang, Haotian Tang, Shang Yang, Wei-Ming Chen, Wei-Chen Wang, Guangxuan Xiao, Xingyu Dang, Chuang Gan, and Song Han. Awq: Activation-aware weight quantization for on-device llm compression and acceleration. *Proceedings of Machine Learning and Systems*, 6:87–100, 2024.
- [28] Yifei Liu, Jicheng Wen, Yang Wang, Shengyu Ye, Li Lyna Zhang, Ting Cao, Cheng Li, and Mao Yang. Vptq: Extreme low-bit vector post-training quantization for large language models. *arXiv preprint arXiv:2409.17066*, 2024.
- [29] Zechun Liu, Changsheng Zhao, Igor Fedorov, Bilge Soran, Dhruv Choudhary, Raghuraman Krishnamoorthi, Vikas Chandra, Yuandong Tian, and Tijmen Blankevoort. Spinqant: Llm quantization with learned rotations. *arXiv preprint arXiv:2405.16406*, 2024.
- [30] Zirui Liu, Jiayi Yuan, Hongye Jin, Shaochen Zhong, Zhaozhuo Xu, Vladimir Braverman, Beidi Chen, and Xia Hu. Kivi: A tuning-free asymmetric 2bit quantization for kv cache. *arXiv preprint arXiv:2402.02750*, 2024.
- [31] Meta. <https://ai.meta.com/blog/meta-llama-3-1/>, 2024.
- [32] Ziran Qin, Yuchen Cao, Mingbao Lin, Wen Hu, Shixuan Fan, Ke Cheng, Weiyao Lin, and Jianguo Li. Cake: Cascading and adaptive kv cache eviction with layer preferences. *arXiv preprint arXiv:2503.12491*, 2025.
- [33] Siva Reddy, Danqi Chen, and Christopher D Manning. Coqa: A conversational question answering challenge. *Transactions of the Association for Computational Linguistics*, 7:249–266, 2019.
- [34] Mark Rudelson and Roman Vershynin. Hanson-wright inequality and sub-gaussian concentration. 2013.
- [35] ShareGPT Team. <https://sharegpt.com/>, 2023.
- [36] Hugo Touvron, Louis Martin, Kevin Stone, Peter Albert, Amjad Almahairi, Yasmine Babaei, Nikolay Bashlykov, Soumya Batra, Prajjwal Bhargava, Shruti Bhosale, et al. Llama 2: Open foundation and fine-tuned chat models. *arXiv preprint arXiv:2307.09288*, 2023.
- [37] Albert Tseng, Jerry Chee, Qingyao Sun, Volodymyr Kuleshov, and Christopher De Sa. QuIP#: Even better LLM quantization with hadamard incoherence and lattice codebooks. In Ruslan Salakhutdinov, Zico Kolter, Katherine Heller, Adrian Weller, Nuria Oliver, Jonathan Scarlett, and Felix Berkenkamp, editors, *Proceedings of the 41st International Conference on Machine Learning*, volume 235 of *Proceedings of Machine Learning Research*, pages 48630–48656. PMLR, 21–27 Jul 2024.
- [38] Ashish Vaswani, Noam Shazeer, Niki Parmar, Jakob Uszkoreit, Llion Jones, Aidan N Gomez, Łukasz Kaiser, and Illia Polosukhin. Attention is all you need. *Advances in neural information processing systems*, 30, 2017.
- [39] Hongyu Wang, Shuming Ma, and Furu Wei. Bitnet v2: Native 4-bit activations with hadamard transformation for 1-bit llms. *arXiv preprint arXiv:2504.18415*, 2025.
- [40] Jason Wei, Xuezhi Wang, Dale Schuurmans, Maarten Bosma, Fei Xia, Ed Chi, Quoc V Le, Denny Zhou, et al. Chain-of-thought prompting elicits reasoning in large language models. *Advances in neural information processing systems*, 35:24824–24837, 2022.
- [41] June Yong Yang, Byeongwook Kim, Jeongin Bae, Beomseok Kwon, Gunho Park, Eunho Yang, Se Jung Kwon, and Dongsoo Lee. No token left behind: Reliable kv cache compression via importance-aware mixed precision quantization. *arXiv preprint arXiv:2402.18096*, 2024.
- [42] Zhihang Yuan, Jiawei Liu, Jiaxiang Wu, Dawei Yang, Qiang Wu, Guangyu Sun, Wenyu Liu, Xinggong Wang, and Bingzhe Wu. Benchmarking the reliability of post-training quantization: a particular focus on worst-case performance. *arXiv preprint arXiv:2303.13003*, 2023.

- [43] Tianyi Zhang, Jonah Yi, Zhaozhuo Xu, and Anshumali Shrivastava. Kv cache is 1 bit per channel: Efficient large language model inference with coupled quantization. *Advances in Neural Information Processing Systems*, 37:3304–3331, 2024.
- [44] Zhenyu Zhang, Ying Sheng, Tianyi Zhou, Tianlong Chen, Lianmin Zheng, Ruisi Cai, Zhao Song, Yuandong Tian, Christopher Ré, Clark Barrett, et al. H2o: Heavy-hitter oracle for efficient generative inference of large language models. *Advances in Neural Information Processing Systems*, 36:34661–34710, 2023.

A Proof for variance bounds of NSN

A.1 Proof of Lemma 1

1. Notation. Write $\mu_i = \mathbb{E}[X_i]$ and $\bar{\varepsilon} = \frac{1}{d} \sum_{i=1}^d \mu_i^2 \leq \varepsilon$. Decompose $\Sigma = \text{Cov}(X) = D + A$, $D = \text{diag}(\Sigma)$, $A_{ii} = 0$, $\|A\|_F \leq \Gamma$.

2. Expected diagonal term. Because $\sum_i \mathbb{E}[X_i^2] = d$,

$$\frac{1}{d} \text{Tr}(D) = \frac{1}{d} \sum_{i=1}^d (\text{Var}(X_i)) = 1 - \bar{\varepsilon}.$$

3. Quadratic form. Choose a Hadamard row $h = \frac{1}{\sqrt{d}}s$, $s \in \{\pm 1\}^d$. Then

$$h^\top D h = 1 - \bar{\varepsilon}, \quad f(h) := h^\top A h = \frac{1}{d} s^\top A s,$$

and $\text{Var}(Y_i) = (1 - \bar{\varepsilon}) + f(h)$. $\mathbb{E}[f(h)] = 0$ since s is randomized with the equal probability of $1/2$.

4. Hanson–Wright Since s is a Rademacher vector, it is a sub-gaussian vector. Applying the Hanson–Wright inequality [34], for any $u > 0$

$$\Pr(|s^\top A s| > u) \leq 2 \exp(-c u^2 / \Gamma^2)$$

where c is a universal constant. Put $u = dt$; then

$$\Pr(|f(h)| > t) \leq 2 \exp(-c d^2 t^2 / \Gamma^2).$$

5. Tail parameter. Choose $t = \Gamma \beta_\alpha$, $\beta_\alpha = \frac{1}{d} \sqrt{\ln(2/\alpha)/c}$. Exponent becomes $-\ln(2/\alpha)$; hence $\Pr(|f(h)| > t) \leq \alpha$.

6. Combine. Since $0 \leq \bar{\varepsilon} \leq \varepsilon$, with probability at least $1 - \alpha$

$$\text{Var}(Y_i) \in [1 - \varepsilon - \Gamma \beta_\alpha, 1 + \Gamma \beta_\alpha].$$

A.2 Off-diagonal Frobenius norms of covariance

To obtain insights regarding the bounds from Lemma 1, we measure the layer-wise average off-diagonal Frobenius norms of covariance matrixs. For key, the covariance is computed right before the Hadamard transform. For value, we remove fused Hadamard transform in the value projection matrix and compute covariance right after the NSN. Note again that the order between adjacent NSN and Hadamard transform is interchangeable. The result is shown in Figure 6. The Frobenius norm is large in the first few layers for both key and value, and remains low in the later layers. This finding is consistent with the pattern observed in Figure 12 and 13, where standardization fails in the early layers. The reason for the large Frobenius norm in the first layers is visualized in Figure 7. For both key and value, there exist outlier values in covariance matrices, leading to the large Frobenius norm.

B Attention computation in NSN

NSNQuant computes the attention weights and outputs using the byproducts from the NSN process. First, the dot product between the query and key is computed as follows:

$$\begin{aligned} qK^T &= q(\text{RoPE}(K_{\text{pre-RoPE}}))^T = q(\text{RoPE}(s_1^k(s_2^k v_{\text{nsn}}^k + o^k)))^T \\ &= q(s_1^k s_2^k \text{RoPE}(v_{\text{nsn}}^k) + s_1^k \text{RoPE}(o^k))^T \\ &= s_1^k s_2^k \text{HT}(q)(\text{HT}(\text{RoPE}(v_{\text{nsn}}^k)))^T + s_1^k q(\text{RoPE}(o^k))^T \\ &\simeq s_1^k s_2^k q_{\text{Had}} v_Q^k + s_1^k q(\text{RoPE}(o^k))^T \end{aligned}$$

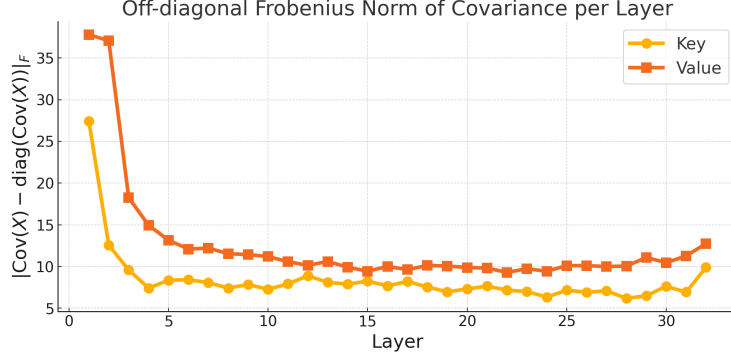


Figure 6: Average off-diagonal Frobenius norm of covariance matrix. The results are measured with LLaMA2-7B on WikiText-2.

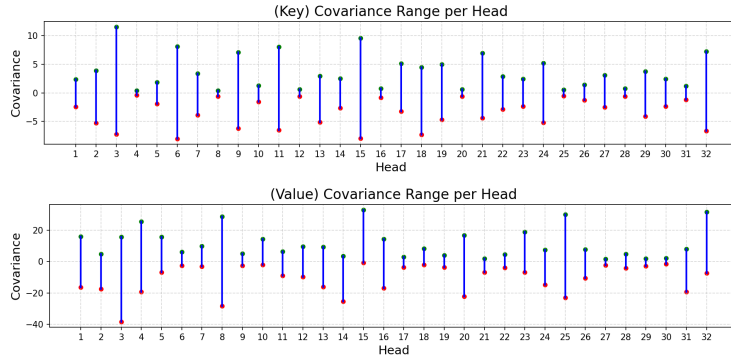


Figure 7: The min-max range of off-diagonal covariances of keys (top) and values (bottom) in the first layer of LLaMA2-7B. Both key and value suffer from outliers in covariance matrices. We use the first sample from the WikiText-2 for visualization.

Here, $\text{HT}(\cdot)$ is the Hadamard transform, and $v_Q^k := \mathbb{C}[\text{VQ}(\text{HT}(\text{RoPE}(v_{\text{nsn}}^k)))]$, $q_{\text{Had}} := \text{HT}(q)$. Since o^k has a different length from K , we expand it within a kernel to match the shape. We obtain attention weights through $W := \text{softmax}(qK^T)$ and then compute the outputs as follows:

$$WV = Ws_1^v(s_2^v v_{\text{nsn}}^v + o^v) \simeq Ws_1^v(s_2^v v_Q^v + o^v), \quad v_Q^v := \mathbb{C}[\text{VQ}(v_{\text{nsn}}^v)].$$

C Additional ablation studies

C.1 Effects of using randomized Hadamard transform (RHT)

From Lemma 1, we find that adopting randomized Hadamard transform after the NSN process gives theoretical bounds to the variance of each channel. However, since the covariances between channels tend to have uniform signs, we find that using the naive Hadamard transform works well enough. As shown in Table 6, both transforms give similar results. Since RHT needs more parameters and computations, we use the naive Hadamard transform in the final design.

Table 6: Perplexity of LLaMA2-7B on WikiText-2 and C4 with NSNQuant-2b using different types of Hadamard transform.

Method	WikiText-2	C4
Hadamard transform	5.285	6.856
RHT	5.290	6.854

C.2 Effects of residual size

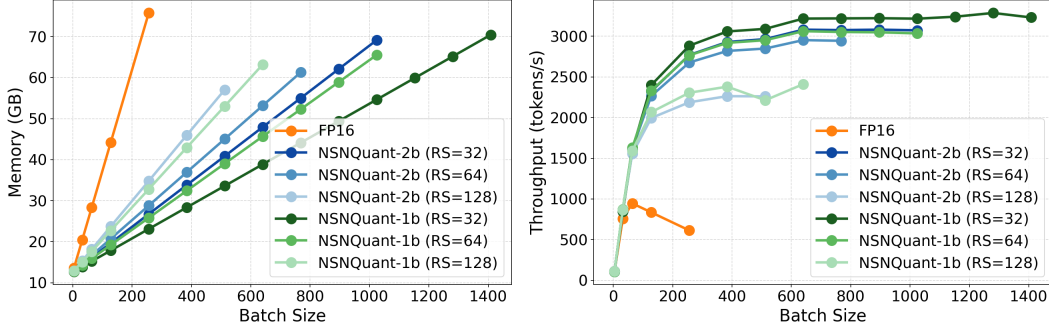


Figure 8: Peak memory usage (left) and throughput (right) measured with varying batch sizes and residual sizes

Table 7: Evaluation results on GSM8K, HumanEval, CoQA, and MMLU with LLaMA3.1-8B-Instruct. RS refers to residual size.

Method	Bits	GSM8K (8-shot, CoT)	HumanEval	CoQA	MMLU (4-shot, CoT)			
					Humanities	STEM	Social	Other
NSNQuant-2b (RS=32)	2.30	74.90	53.05	63.83	70.24	56.56	74.22	70.98
NSNQuant-2b (RS=64)	2.23	75.89	56.10	63.83	71.04	55.64	73.42	70.74
NSNQuant-2b (RS=128)	2.19	75.66	56.71	62.93	69.29	57.38	74.49	70.80
NSNQuant-1b (RS=32)	1.30	42.08	42.07	63.67	59.47	44.88	65.95	63.42
NSNQuant-1b (RS=64)	1.23	53.45	44.51	62.70	59.82	45.83	65.34	63.77
NSNQuant-1b (RS=128)	1.19	57.54	48.17	63.88	61.77	49.07	67.63	66.86

We fix the residual size to 64 in our main experiments, for fair evaluation across different methods. However, the residual size is an important hyperparameter that determines the number of full precision caches. Therefore, we evaluate NSNQuant with 3 different residual sizes—32, 64, 128—with LLaMA3.1-8B-Instruct. Since LongBench is not effective to show performance differences in 2-bit regime, we use GSM8K, HumanEval, and CoQA. The result is shown in Table 7. For NSNQuant-1b, we observe that performance is highly sensitive to the choice of residual size. A residual size of 128 yields the best results across most benchmarks, while a residual size of 32 performs the worst. In contrast, NSNQuant-2b shows comparable performance with different residual sizes. These results suggest that NSNQuant-2b produces higher-quality quantizations, making it more robust to variations in residual size.

We also report the memory usage and throughput with different residual sizes in Figure 8. The result shows that the methods with smaller residual sizes require less memory and achieve higher throughput. Note that the impact of residual size to memory and throughput will decrease as the sequence length gets longer.

C.3 Effects of scale adjustment

Motivating Example Suppose we are quantizing a 2-dimensional vector $(1, 2)$ using a codebook with two entries: $(0.8, 1.6)$ and $(2, 3)$. The vector would be approximated by $(0.8, 1.6)$, incurring a non-negligible error. However, this error could be significantly reduced by scaling the quantized vector by a factor of 1.25.

As this example illustrates, using the quantized vector v_Q without any scaling leads to suboptimal approximation. To identify a more effective scaling strategy, we evaluate three probable approaches, as visualized in Figure 9. The first approach is to scale v_Q to minimize the L2 error between v and v_Q , the second approach is to scale v_Q to match the size of v , and the third approach is to scale v_Q to preserve components parallel to v . The result of applying three strategies is presented in Table 8. For both key and value, strategy 3 shows the best quantization quality. By applying it to both key and

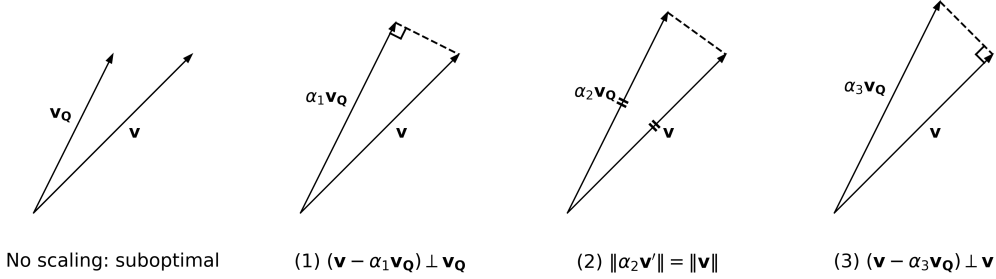


Figure 9: Visualization of the three tested scale adjustment strategies.

Table 8: Perplexity of LLaMA2-7B on WikiText-2 under different scaling strategies for key and value. NSNQuant-2b is used here for ablation.

Strategy	PPL
No scaling	5.395
Key - Strategy 1	5.378
Key - Strategy 2	5.329
Key - Strategy 3	5.317
Value - Strategy 1	5.394
Value - Strategy 2	5.355
Value - Strategy 3	5.335
Key - Strategy 3 + Value - Strategy 3	5.285

value in NSNQuant-2b, the perplexity of LLaMA2-7B on WikiText-2 is reduced from 5.395 to 5.285.

C.4 Effects of codebook tuning

Table 9: Perplexity of LLaMA2-7B on WikiText-2 using different codebooks.

Method	Codebook	PPL
NSNQuant-2b	K-Means	5.294
	E8P	5.284
	K-Means + Fine-tuning	<u>5.285</u>
NSNQuant-1b	K-Means	6.910
	K-Means + Fine-tuning	6.703

As mentioned in section 3.4, we propose to fine-tune a codebook obtained from the K-Means algorithm. Since the error of scale adjustment only depends on the angle between v and v_Q , we set the objective to minimize the cosine distance between them. The perplexity result with LLaMA2-7B on WikiText-2 is presented in Table 9. The result shows that fine-tuning improves quantization quality in both NSNQuant-1b and NSNQuant-2b, and matches the performance of E8P [37] in 2-bit quantization.

C.5 Effects of pre-RoPE NSN

As visualized in Figure 2, NSNQuant applies NSN to keys before the RoPE. However, it seems natural to apply NSN after RoPE since RoPE may induce noises to the channel-wise mean. The PPL evaluation results in both settings are presented in Table 10. The pre-RoPE NSN achieves slightly lower PPL than the post-RoPE NSN. We attribute this to two reasons. First, the effect of RoPE on the channel-wise mean is minimal, as the tokens within the residual share the similar rotating angles. Second, computing full-precision RoPE for o is beneficial, since the RoPE rotation matrix contains important position information.

Table 10: Perplexity of LLaMA2-7B and LLaMA2-13B on WikiText-2 with NSNQuant-2b using different locations of NSN.

Normalization	LLaMA2-7B	LLaMA2-13B
pre-RoPE NSN	5.29	4.71
post-RoPE NSN	5.33	4.73

C.6 Effects of double quantization

Table 11 shows the performance change when applying double quantization. The performance degradation is minimal, while the memory savings are substantial.

Table 11: Impact of double quantization on the perplexity of LLaMA2-7B on WikiText-2, using NSNQuant-2b for ablation.

Method	Avg. bit width	PPL
Baseline	2.5	5.278
+ Codebook Double Quantization	2.5	5.280
+ Mean Double Quantization	2.33	5.287
+ Scale Double Quantization	2.23	5.285

D Variants of NSN

D.1 Replacing the Shift step with Weiszfeld algorithm

As noted in Section 3.2, the final normalization step of NSN can introduce a small bias, leaving the channel-wise mean slightly off zero. To verify that it barely affects the quantization quality, we provide a mathematical explanation and an experiment where we totally remove such bias by adopting Weiszfeld algorithm.

First, here is an intuitive explanation of why the small bias introduced by the last step of NSN does not significantly affect the quantization error. Let $v_n = \{v_1, v_2, \dots, v_l\} \in \mathbb{R}^{l \times d}$ denote the output tokens after the first normalization step. Since the next step, **Shift**, subtracts the mean, we have $v_{ns} = \{v_1 - \mathbb{E}[v_i], v_2 - \mathbb{E}[v_i], \dots, v_l - \mathbb{E}[v_i]\}$. **(i)** If $\text{Var}[v_i]$ is small, then $\mathbb{E}[(v_i - \mathbb{E}[v_i])^2]$ is also small. Since we save $o = \mathbb{E}[v_i]$ in full-precision, the fact that the norm of the leftover part $(v_i - \mathbb{E}[v_i])$ is small implies that the final error will also be small. **(ii)** If $\text{Var}[v_i]$ is large, then $\mathbb{E}[v_i]$ will be small because $\mathbb{E}[v_i]^2 = \mathbb{E}[v_i^2] - \text{Var}[v_i] = d - \text{Var}[v_i]$. Small $\mathbb{E}[v_i]$ means that the token-wise norm will not change much, and the last step will not significantly affect the channel-wise mean. To conclude, regardless of the magnitude of $\text{Var}[v_i]$, the final quantization error would remain small because either the alignment is well preserved, or the leftover magnitude is small.

Second, to empirically explore the impact of removing this drift, we reformulate the second step (Shift) as the search for the geometric median. Let $\{t_i\}_{i=1}^{rs} \subset \mathbb{R}^d$ denote the tokens in a group of residual size after the first normalization step. We seek o_* such that

$$\mathcal{L}(o) := \sum_{i=1}^{rs} \frac{t_i - o}{\|t_i - o\|} = \mathbf{0}. \quad (2)$$

Setting $F(o) := \sum_{i=1}^{rs} \|t_i - o\|$ gives $\nabla F(o) = \mathcal{L}(o)$; hence any o satisfying (2) minimizes F and is the geometric median of the set $\{t_i\}$.

We compute o_* with the Weiszfeld algorithm—the standard iterative solver for geometric medians—and subtract it instead of the arithmetic mean in NSN’s second step. The resulting variant keeps the post-normalization mean essentially at zero. Table 12 presents the perplexity evaluation results on WikiText-2 and C4 with LLaMA-2-7B. The change yields only marginal negative effects despite the additional cost from the iterative updates. Hence, we keep the original mean-subtraction step in the final NSN design.

]

Table 12: Perplexity of LLaMA2-7B on WikiText-2 and C4 with NSNQuant-2b using different normalization strategies.

Normalization	WikiText-2	C4
NSN	5.285	6.856
N-Weiszfeld-N	5.289	6.863

D.2 Replacing the second Normalization step with channel-wise scaling

A straightforward way to standardize the output distribution is to simply shift and scale in a channel dimension. Therefore, we try replacing our third step—token-wise normalization—with channel-wise scaling, where sample standard deviation is divided from each channel. We also move the location of normalizations next to the Hadamard transform so that it does not affect channel-wise statistics. The result is shown in Table 13. Using channel-wise scaling instead of token-wise normalization is not as effective as token-wise normalization. This is because channel-wise scaling does not suppress outlier tokens, especially the attention sink token. For example, using the first sample from WikiText-2 dataset, the average norm of the first token in the first layer is 19.1, which is nearly twice as large as the overall average (11.3). Considering a ball-shaped property of our codebook, quantization error would be large for these tokens since their magnitudes are far from zero. On the other hand, our token-wise normalization effectively regulates the scale, making our codebook work effectively.

Table 13: Perplexity of LLaMA2-7B on WikiText-2 and C4 with NSNQuant-2b using different normalization strategies

Normalization	WikiText-2	C4
NSN	5.285	6.856
NS-Channel-wise Scaling	6.251	8.265

E Experiment details

E.1 Experiment environments

The PPL evaluation is performed on a Linux server with 2 RTX Titan GPUs. The evaluations on LongBench, GSM8K, HumanEval, CoQA, MMLU are conducted on a Linux server with 8 RTX 3090 GPUs. Efficiency analysis is conducted on a Linux server with a single A100-80GB GPU. All methods are implemented based on the HuggingFace Transformers library using PyTorch framework.

E.2 LongBench evaluation metrics

Table 14 shows the evaluation metrics used in LongBench. Qasper, TREC, and TriviaQA use exact matching-based metrics, while the other tasks use heuristic metrics.

Table 14: Evaluation metrics used in LongBench evaluation

Task	Evaluation Metric
Qasper	F1
QMSum	ROUGE-L
MultiNews	ROUGE-L
TREC	Accuracy
TriviaQA	F1
SAMSum	ROUGE-L
LCC	Edit Sim
RepoBench-P	Edit Sim

E.3 Additional explanation on baselines

KIVI [30] is one of the pioneering works in low-bit quantization of the KV cache of LLMs. KIVI quantizes key cache along the channel dimension and value cache along the token dimension, considering its outlier patterns. To maintain the consistency with our residual policy, we use group size of 64 for keys. Also, since smaller group sizes incur large additional bits which is critical for low-bit scenario, we use 128 for values.

KIVI + Had is a variant of KIVI, where the Hadamard transform for key and value is added to the existing KIVI framework. We add this variant because Hadamard transform is known to reduce errors in token-wise quantization a lot, especially in a round-to-nearest (RTN)-based method like KIVI.

KVQuant [19] is another pioneering work in KV cache quantization. Similar to KIVI, KVQuant quantizes key and value cache along the channel dimension and token dimension, respectively. KVQuant employs non-uniform quantization (nuq) and dense-and-sparse quantization to improve performance further. We apply Q-Norm and 1% dense-and-sparse quantization to both KVQuant-1b and KVQuant-2b to obtain the best result.

CQ [43] is our main competitor, which shares the core idea of VQ. CQ quantizes grouped channels using learned centroids, which serve as a codebook. We evaluate the performance of CQ-4c9b for 2-bit quantization, and CQ-8c10b for 1-bit quantization.

E.4 LM-Eval tasks

For evaluation on GSM8K, HumanEval, CoQA, and MMLU, we use the following tasks provided in lm-evaluation-harness [13]: `gsm8k_cot`, `humaneval`, `coqa`, `mmlu_flan_cot_fewshot_humanities`, `mmlu_flan_cot_fewshot_stem`, `mmlu_flan_cot_fewshot_social_sciences`, `mmlu_flan_cot_fewshot_other`.

F Additional results

F.1 PPL evaluation in generation setting

Since the perplexity (PPL) evaluation in Table 2 is different from our generation setting, we provide PPL evaluation results in the generation setting. We obtain the output logits by processing tokens one-by-one, just like in a generation scenario. We also adopt residuals to maintain recent tokens in full-precision. The result is presented in Table 15. All methods achieve lower PPLs compared to the results in Table 2 because of the residual, but their relative order has similar trends. Since the PPL evaluation setting in the main table is much more efficient to measure and closer to convention in the previous studies, we use the same setting in the ablation studies.

F.2 Additional results on LongBench

Table 16 presents evaluation results on LongBench with LLaMA2-7B-Chat and LLaMA3-8B-Instruct. Similar to the main table, NSNQuant-1b outperforms other 1-bit quantization methods by a large margin. However, 2-bit results are quite noisy, without any clear trend. For example, KVQuant-2b struggles in LLaMA2-7B-Chat, but achieves the best score in LLaMA3-8B-Instruct. This is another example that shows the noisiness of metrics. As shown in Table 16, KVQuant-2b achieves 56.51 in RepoBench-P, which is much higher than that of FP16. This result is unreliable since KVQuant suffers from performance degradation in other tasks.

To reduce the impact of noisiness, we evaluate each method in a different perspective: how well each method preserves the original outputs. To achieve this, we measure the ROUGE-L score of each method by comparing their outputs with FP16 outputs. Since Qasper, TREC, and TriviaQA are evaluated using exact matching-based metrics, we exclude them from the task list. The result is shown in Table 17. It clearly shows that NSNQuant is the most effective method which preserves the original output faithfully. On the other hand, CQ is even worse than KIVI + Had, suggesting that calibration-based VQ suffers from significant performance degradation when applied to diverse tasks.

Table 15: Perplexity evaluated in generation setting with residual, for different models on WikiText-2 and C4.

Method	Avg. bit width	Dataset	LLaMA2-7B	LLaMA3.1-8B
FP16	16	C4	7.04	10.36
		WikiText-2	5.42	7.04
KIVI-2	2.38	C4	6.63	8.43
		WikiText-2	5.12	5.84
KIVI-2 + Had	2.38	C4	6.88	9.56
		WikiText-2	5.30	6.68
KVQuant-2b + 1%	2.32	C4	6.84	8.88
		WikiText-2	5.32	6.20
CQ-4c9b	2.26	C4	6.84	9.48
		WikiText-2	5.22	6.00
NSNQuant-2b	2.23	C4	6.69	8.69
		WikiText-2	5.16	6.03
KVQuant-1b + 1%	1.32	C4	9.67	16.05
		WikiText-2	6.70	12.02
CQ-8c10b	1.27	C4	7.61	20.33
		WikiText-2	5.56	6.53
NSNQuant-1b	1.23	C4	7.07	10.32
		WikiText-2	5.48	7.55

Table 16: Additional results on LongBench with LLaMA2-13B-Chat, LLaMA2-7B-Chat and LLaMA3-8B-Instruct

Model	Method	Bits	Qasper	QMSum	MultiNews	TREC	TriviaQA	SAMSum	LCC	RepoBench-P	Avg.
LLaMA2-13B-Chat	FP16	16	17.06	20.95	26.55	68.50	87.75	42.59	48.27	49.80	45.18
	KIVI-2	2.38	17.44	20.53	26.03	67.00	87.39	41.79	46.54	47.33	44.26
	KIVI-2 + Had	2.38	15.44	19.59	26.19	68.00	86.55	41.93	48.22	50.10	44.50
	KVQuant-2b + 1%	2.32	16.57	19.72	25.59	68.00	88.07	40.72	47.64	49.70	44.50
	CQ-4c9b	2.26	18.42	19.72	25.12	67.00	87.69	41.32	47.18	48.32	44.35
	NSNQuant-2b	2.23	17.28	20.41	26.16	68.50	87.51	42.48	47.82	49.69	44.98
	KVQuant-1b + 1%	1.32	13.85	18.32	20.11	46.50	81.67	29.60	35.46	32.78	34.79
	CQ-8c10b	1.27	16.08	18.67	20.87	49.00	87.12	37.44	43.17	42.34	39.34
	NSNQuant-1bit	1.23	17.98	20.56	25.92	67.50	87.17	41.08	48.19	50.10	44.81
LLaMA2-7B-Chat	FP16	16	21.95	20.71	26.21	64.00	83.09	41.39	58.31	52.16	45.98
	KIVI-2	2.38	24.69	20.83	25.99	63.50	83.05	40.57	56.69	49.90	45.65
	KIVI-2 + Had	2.38	20.62	21.03	25.98	64.00	83.45	41.11	56.79	51.10	45.51
	KVQuant-2b + 1%	2.33	20.84	21.22	24.89	62.50	83.82	39.87	55.48	49.73	44.79
	CQ-4c9b	2.26	20.73	20.64	24.92	63.00	84.14	39.90	57.63	51.30	45.28
	NSNQuant-2b	2.23	22.01	20.87	26.42	64.00	83.67	40.51	57.71	51.47	45.83
	KVQuant-1b + 1%	1.32	13.10	20.27	20.82	30.00	61.43	34.14	43.16	39.31	32.78
	CQ-8c10b	1.27	14.82	19.82	20.48	42.00	82.49	36.62	49.45	46.60	39.04
	NSNQuant-1b	1.23	17.70	20.74	25.49	64.00	82.06	40.31	55.14	50.57	44.50
LLaMA3-8B-Instruct	FP16	16	31.25	23.54	26.69	74.00	90.31	42.65	57.23	51.69	49.67
	KIVI-2	2.38	20.92	23.82	26.34	74.00	90.08	40.87	46.64	46.87	46.19
	KIVI-2 + Had	2.38	23.93	22.58	26.35	74.00	90.01	41.38	49.97	47.11	46.92
	KVQuant-2b + 1%	2.32	27.91	23.16	25.26	74.00	90.33	39.95	56.50	56.51	49.20
	CQ-4c9b	2.26	26.26	22.60	25.10	73.50	90.78	40.48	57.89	53.28	48.74
	NSNQuant-2b	2.23	29.83	22.66	26.28	74.00	90.31	41.73	55.88	50.31	48.88
	KVQuant-1b + 1%	1.32	13.01	21.45	21.39	61.50	86.12	34.23	47.89	45.96	41.44
	CQ-8c10b	1.27	15.23	21.04	21.63	44.50	87.26	36.63	51.24	46.36	40.49
	NSNQuant-1b	1.23	18.04	21.57	26.36	73.50	90.46	41.06	45.50	42.19	44.84

Table 17: Average ROUGE-L score measured with FP16 output. Qasper, TREC and TriviaQA are excluded since these tasks provide the objective metrics based on exact matching.

Model	Method	Bits	QMSum	MultiNews	SAMSum	LCC	RepoBench-P	Avg.
LLaMA2-13B-Chat	KIVI	2.38	52.34	52.18	73.17	52.51	49.06	55.85
	KIVI + Had	2.38	55.24	55.39	76.53	60.55	57.24	60.99
	KVQuant-2b + 1%	2.32	55.85	53.02	76.55	57.07	53.91	59.28
	CQ-4c9b	2.26	56.07	50.77	74.61	54.85	49.19	57.10
	NSNQuant-2b	2.23	62.73	59.69	85.02	70.93	68.23	69.32
	KVQuant-1b + 1%	1.32	40.88	32.00	42.86	22.95	18.32	31.40
	CQ-c8b10	1.27	43.39	34.49	59.21	30.59	26.41	38.82
	NSNQuant-1b	1.23	51.63	51.12	71.77	52.94	48.44	55.18
LLaMA2-7B-Chat	KIVI	2.38	46.95	48.04	67.22	47.32	46.96	51.30
	KIVI + Had	2.38	49.12	50.13	73.87	55.30	56.36	56.95
	KVQuant-2b + 1%	2.32	50.77	47.71	74.73	55.20	55.24	56.73
	CQ-4c9b	2.26	52.04	47.19	69.22	50.70	48.80	53.59
	NSNQuant-2b	2.23	58.19	55.42	80.14	69.93	67.36	66.21
	KVQuant-1b + 1%	1.32	37.66	33.14	44.16	22.34	23.54	32.17
	CQ-c8b10	1.27	40.01	31.07	56.00	25.52	27.02	35.92
	NSNQuant-1b	1.23	46.42	47.91	66.08	47.65	46.92	51.00
LLaMA3-8B-Instruct	KIVI	2.38	49.38	48.54	44.29	44.45	40.33	45.40
	KIVI + Had	2.38	49.35	51.77	46.83	49.65	46.67	48.85
	KVQuant-2b + 1%	2.32	50.60	50.00	45.66	53.18	46.14	49.12
	CQ-4c9b	2.26	50.06	47.76	49.25	49.65	41.63	47.67
	NSNQuant-2b	2.23	57.24	57.02	55.29	65.43	60.09	59.01
	KVQuant-1b + 1%	1.32	37.22	31.72	29.58	25.71	22.70	29.39
	CQ-c8b10	1.27	37.92	32.27	34.20	28.07	22.25	30.94
	NSNQuant-1b	1.23	44.00	48.31	41.04	42.99	36.17	42.50
LLaMA3.1-8B-Instruct	KIVI	2.38	45.23	47.48	42.19	52.31	43.98	46.24
	KIVI + Had	2.38	47.75	50.65	44.11	57.71	51.76	50.40
	KVQuant-2b + 1%	2.32	46.33	49.32	45.85	57.20	52.07	50.15
	CQ-4c9b	2.26	45.45	48.54	47.76	54.13	45.55	48.29
	NSNQuant-2b	2.23	51.72	56.69	52.27	68.32	64.37	58.67
	KVQuant-1b + 1%	1.32	34.62	33.02	32.44	26.67	22.68	29.89
	CQ-c8b10	1.27	33.70	32.47	29.32	29.36	22.30	29.43
	NSNQuant-1b	1.23	41.92	46.91	40.68	46.85	37.56	42.78
Mistral-7B-Instruct-v0.3	KIVI	2.38	50.56	49.99	78.84	61.02	49.35	57.95
	KIVI + Had	2.38	56.40	55.62	79.54	65.26	57.83	62.93
	KVQuant-2b + 1%	2.32	53.09	51.12	77.38	64.04	56.96	60.52
	CQ-4c9b	2.26	52.58	51.55	80.26	60.15	52.80	59.46
	NSNQuant-2b	2.23	63.19	60.06	84.42	75.32	69.85	70.57
	KVQuant-1b + 1%	1.32	36.65	32.30	60.32	34.81	28.97	38.61
	CQ-c8b10	1.27	39.17	33.26	64.46	34.86	27.29	39.81
	NSNQuant-1b	1.23	49.96	50.01	74.29	55.03	45.03	54.86

F.3 Additional results on GSM8K, HumanEval, CoQA, and MMLU

Table 18 presents the additional results for GSM8K, HumanEval, CoQA, and MMLU. The result shows a similar trend to Table 4, where NSNQuant generally outperforms other methods in both 1-bit and 2-bit quantization.

F.4 Results on AIME-2024

To evaluate the long-context reasoning ability, we evaluate our methods on AIME-2024, with DeepSeek-R1-Distill-Llama-8B. As suggested in DeepSeek [15], we set temperature to 0.6, top-p to 0.95, and max generated tokens to 32768. Since AIME-2024 only contains 30 problems, we run evaluation with 5 different seeds.

The result is shown in Table 19. In 2-bit quantization, NSNQuant and CQ both show little accuracy drop with small differences. On the other hand, under 1-bit quantization, both methods experience significant performance degradation, but NSNQuant-1b achieves over $2\times$ higher accuracy than CQ-8c10b. While CQ-4b9c is generally strong in math reasoning tasks such as GSM-8K and AIME-2024, CQ-8b10c fails severely in such datasets.

Table 18: Additional results on GSM8K, HumanEval, CoQA, and MMLU with LLaMA2-13B-Chat and LLaMA3-8B-Instruct.

Model	Method	Bits	GSM8K (8-shot, CoT)	HumanEval	CoQA	MMLU (4-shot, CoT)			
						Humanities	STEM	Social	Other
LLaMA2-13B-Chat	FP16	16	37.30	17.07	64.08	60.89	41.54	62.54	60.95
	KIVI	2.38	30.63	15.24	63.70	57.48	38.66	57.42	56.21
	KIVI + Had	2.38	31.69	14.02	63.03	59.91	<u>40.21</u>	<u>61.05</u>	<u>59.25</u>
	KVQuant-2b + 1%	2.32	32.98	<u>15.85</u>	64.82	59.15	39.31	59.64	57.96
	CQ-4c9b	2.26	<u>34.04</u>	14.63	<u>64.60</u>	56.26	35.70	57.94	55.47
	NSNQuant-2b	2.23	35.48	18.29	63.67	<u>59.16</u>	41.47	62.34	60.26
	KVQuant-1b + 1%	1.32	8.64	9.15	57.08	<u>29.89</u>	<u>23.14</u>	<u>35.90</u>	<u>21.44</u>
	CQ-8c10b	1.27	<u>19.71</u>	<u>12.20</u>	<u>60.88</u>	21.95	11.25	30.84	19.33
	NSNQuant-1b	1.23	26.84	14.02	63.10	56.43	38.15	58.00	57.71
LLaMA3-8B-Instruct	FP16	16	76.72	28.05	61.47	70.51	53.00	70.89	70.66
	KIVI	2.38	65.35	22.56	60.42	59.18	44.14	61.82	61.73
	KIVI + Had	2.38	69.75	32.93	<u>60.72</u>	63.56	47.36	63.05	65.06
	KVQuant-2bit + 1%	2.32	70.74	23.78	60.30	<u>64.94</u>	46.34	<u>64.67</u>	<u>66.11</u>
	CQ-4c9b	2.26	<u>72.55</u>	23.78	60.60	63.86	<u>47.94</u>	64.20	65.26
	NSNQuant-2bit	2.23	74.53	32.93	61.62	68.95	52.44	69.36	68.91
	KVQuant-1b + 1%	1.32	6.97	<u>14.02</u>	51.28	11.21	13.73	31.25	<u>26.97</u>
	CQ-8c10b	1.27	<u>24.26</u>	13.41	<u>53.38</u>	<u>22.05</u>	<u>14.44</u>	<u>26.42</u>	16.14
	NSNQuant-1bit	1.23	61.64	29.27	60.28	58.73	42.70	59.76	60.94

Table 19: Evaluation results on AIME-2024 with DeepSeek-R1-Distill-Llama-8B

Method	pass@1
FP16	43.3
CQ-4c9b	40.7
NSNQuant-2b	40.0
CQ-8c10b	6.7
NSNQuant-1b	16.7

F.5 Comparison with QuaRot and SpinQuant

QuaRot [2] and SpinQuant [29] are the recent quantization methods for KV cache which also leverage the Hadamard transform. However, we don’t include them as our baselines because they are not suitable for low-bit quantization. Their evaluation results on GSM8K, HumanEval, CoQA, and MMLU with LLaMA3.1-8B-Instruct are shown in Table 20. We use a clipping ratio of 0.95, following QuaRot, and use a group size of 128 for both keys and values. We only train R2 rotation matrix in SpinQuant, since we don’t apply quantization to weights or activations. We also apply the residual policy of NSNQuant, following the setting in the main experiments. The result shows that QuaRot and SpinQuant underperform in every dataset, and they are worse than our weakest baseline, KIVI-2.

Table 20: Evaluation results on GSM8K, HumanEval, CoQA, and MMLU with LLaMA3.1-8B-Instruct.

Method	Bits	GSM8K (8-shot, CoT)	HumanEval	CoQA	MMLU (4-shot, CoT)			
					Humanities	STEM	Social	Other
KIVI-2	2.38	<u>64.59</u>	<u>48.17</u>	63.60	<u>64.44</u>	<u>50.09</u>	<u>66.84</u>	<u>66.1</u>
QuaRot (W16A16KV2)	2.25	<u>48.67</u>	47.56	64.05	57.32	41.91	62.64	60.51
SpinQuant (W16A16KV2)	2.25	41.09	40.24	62.52	56.30	39.53	59.85	59.39
NSNQuant-2b	2.23	75.89	56.10	<u>63.83</u>	71.04	55.64	73.42	70.74

G Visualizations

G.1 Inter-channel correlation after the NSN and Hadamard

We verify that the NSN and Hadamard transform align each channel distribution with the standard normal distribution. However, large inter-channel dependency can change its multi-dimensional shapes, affecting the efficiency of our tuned codebooks. Figure 10 shows the layer-wise mean absolute correlation (MAC) between channels after the NSN and Hadamard transform. Using WikiText-2 and LLaMA2-7B model, we measure the correlations between different channels which are grouped and quantized together. The results show that the correlation is generally small except for the early layers. This indicates our codebook is close to optimal in the later layers, while there is still room for improvement in the early layers.

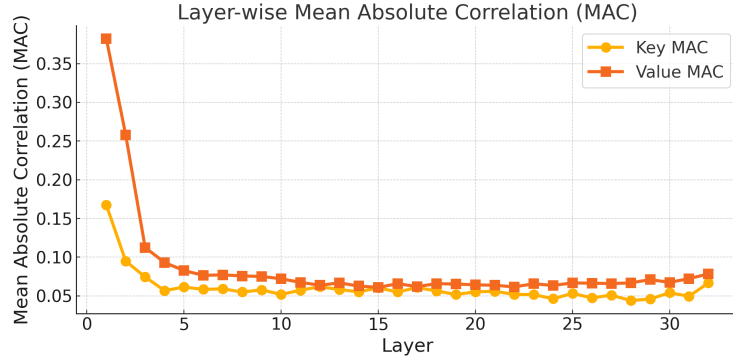


Figure 10: Layer-wise mean absolute correlation (MAC) between different channels. The results are measured on WikiText2 with LLaMA2-7B.

G.2 t-SNE visualization of keys and values

To visualize the divergent token distribution of different datasets, we plot 2D t-SNE results in Figure 11. For MultiNews, LCC, and SAMSum, the "context" column is used for visualization. We sample first 10 samples in the test split for each datasets. The input length is limited to 2048 tokens, resulting in ~ 20000 tokens per dataset. We run t-SNE for all tokens, and randomly select 2000 tokens from each dataset for plotting. None of the normalization methods or rotations are applied to keys and values in this visualization and pre-RoPE keys are used for visualization.

G.3 Channel-wise mean and standard deviation

We visualize the channel-wise mean and standard deviation of keys and values after the NSN and Hadamard transform in Figure 12 and 13. Although mean and standard deviation are generally close to 0 and 1 as expected, there are non-negligible errors in some of the heads in the early layers.

H Latency Measurements

NSNQuant introduces additional computations for normalization, averaging, and shift operations. To assess the overhead, we measure the inference latency under the following setting: a batch size of 32 and an input length of 512. We set the residual size to 64 and generate 64 tokens to ensure that vector quantization is performed exactly once. Latency is measured on a Linux server equipped with a single A100-80GB GPU. Each measurement is repeated 100 times, and the average elapsed time is reported. As shown in Table 21, NSNQuant incurs approximately a 37% increase in inference time during the prefilling stage. In contrast, decoding is significantly faster, as NSNQuant substantially reduces the overhead caused by intensive memory access.

Table 21: Inference latency comparison between the baseline and NSNQuant. We report the average elapsed time over 100 runs on a single A100-80GB GPU. While NSNQuant introduces moderate overhead during the prefilling stage due to additional computations, it achieves faster decoding by alleviating memory access bottlenecks.

Method	Prefill	Decode
FP16	1.229s	0.0507s
NSNQuant-2b	1.675s	0.0324s
NSNQuant-1b	1.698s	0.0324s

I Comparison with CQ

Motivation Although CQ and NSNQuant both quantize multiple channels jointly, their motivations behind adopting vector quantization (VQ) differ. CQ employs VQ to capture correlations across channels, whereas NSNQuant is inspired by the observation from QuIP# [37] that VQ performs particularly well when quantizing ball-shaped vectors. Since the channel distribution is aligned with the standard normal distribution regardless of model and data, we can build an optimized codebook for compressing the normal distribution data in advance.

Calibration CQ requires calibration data and backward passes through model weights to compute Fisher information. In contrast, NSNQuant does not require any external data, and its codebook tuning can be completed within a few minutes on a single GPU. Moreover, the tuned codebook is model-agnostic: it can be reused across models as long as the hidden dimension per head remains unchanged. This property makes NSNQuant much easier to integrate and significantly improves its generalization ability.

Codebook CQ requires a separate codebook for each group of coupled channels. For example, in CQ-8c10b, the total size of all codebooks matches the KV cache for 1024 tokens in fp16, which is equivalent to 16384 tokens in 1-bit representation. In contrast, NSNQuant uses a single shared codebook for the entire model, resulting in almost no additional memory overhead.

J Related Work

Recent efforts to reduce the memory and latency bottlenecks of LLMs have largely focused on weight quantization and KV cache compression. Weight quantization methods such as GPTQ [12] and AWQ [27] significantly reduce the memory footprint of model weights while preserving accuracy. In particular, vector quantization (VQ) methods like QuIP#[37], AQLM[11], and VPTQ [28] enable extremely low-bit quantization of model weights. However, these approaches do not mitigate the growing memory consumption of the KV cache, which scales linearly with sequence length and model depth during long-context inference.

To address this, recent studies have explored compressing the KV cache. KVQuant [19] and KIVI [30] observe the presence of outlier patterns in KV representations and propose to apply channel-wise quantization for key and token-wise quantization for value. CQ [43] extends non-uniform quantization (nuq) to multiple channels, achieving effective 1-bit KV cache compression. Orthogonal approaches, such as H2O [44] and SnapKV [25], reduce memory through cache eviction of uninformative tokens. Hybrid strategies like ZipCache [17] and MiKV [41] selectively maintain high-precision cache for important tokens while applying low-bit quantization elsewhere. Our method uses the same precision for all tokens, but future work could incorporate token importance as in hybrid approaches.

K Limitation and broader impacts

K.1 Limitation

Although proposed Normalize-Shift-Normalize (NSN) is empirically proven to align the output distribution with the standard normal distribution, we find that it does not work well in the early layers due to outlier channels with huge variances. Our analysis shows that the quantization errors in these

layers still remain low, but handling these channels properly will further improve performance. Also, NSNQuant does not consider inter-channel correlations or dependencies, while CQ induces errors by relying too much on them. Exploring a middle ground between two methods will be beneficial: exploiting inter-channel relations, while avoiding overfitting to calibration datasets.

K.2 Broader impacts

Our work improves the scalability and efficiency of LLM inference by reducing memory usage and increasing throughput. This enables broader adoption of LLMs across diverse applications and hardware setups. By significantly reducing memory consumption for long-context inference, our method makes advanced use cases like long-context reasoning feasible even on devices with constrained memory resources.

That said, our work does not provide any empirical analysis regarding safety aspects. As a result, applying quantization may introduce unintended effects such as hallucinations or degraded reliability, especially in sensitive scenarios. We therefore advise caution when deploying quantized models in safety-critical applications.

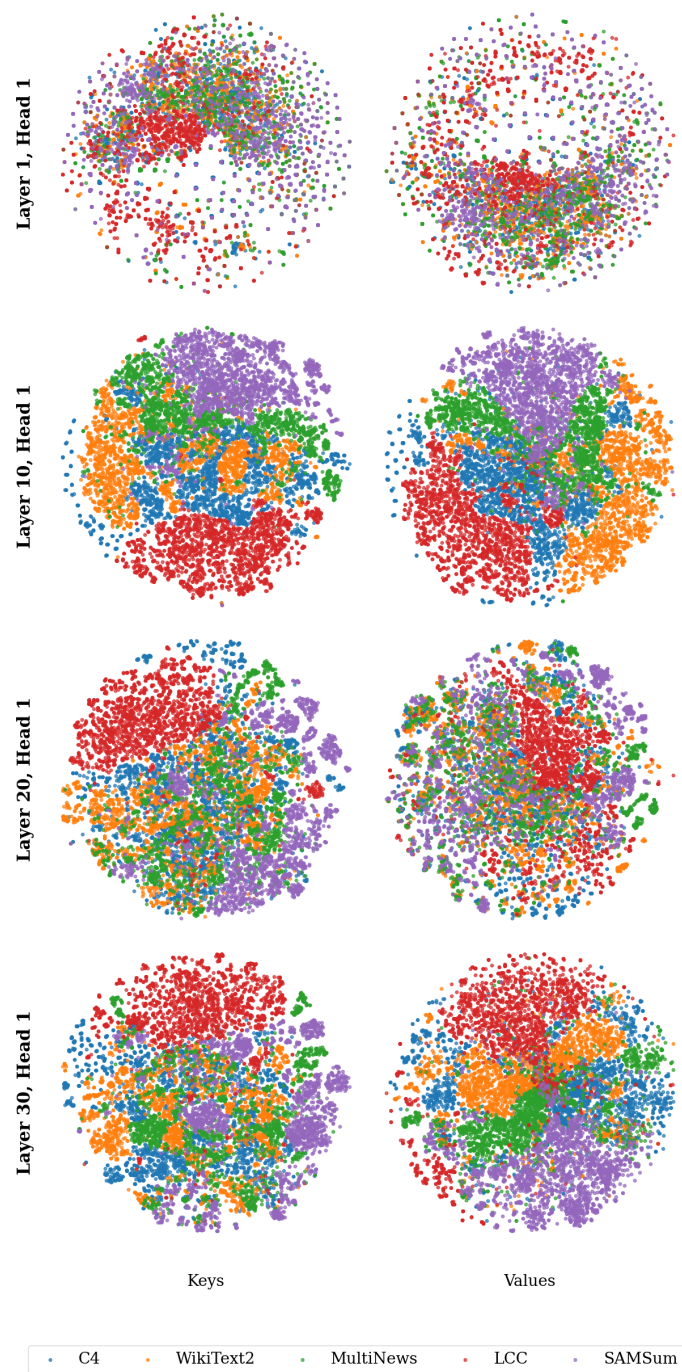
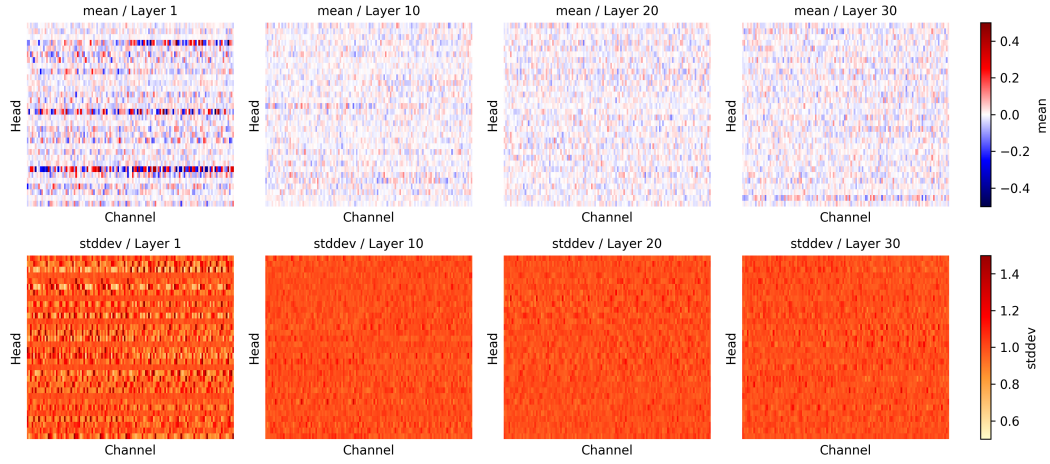


Figure 11: t-SNE visualization LLaMA3.1-8B key and value.

Channel-wise mean / stddev on WikiText-2



Channel-wise mean / stddev on C4

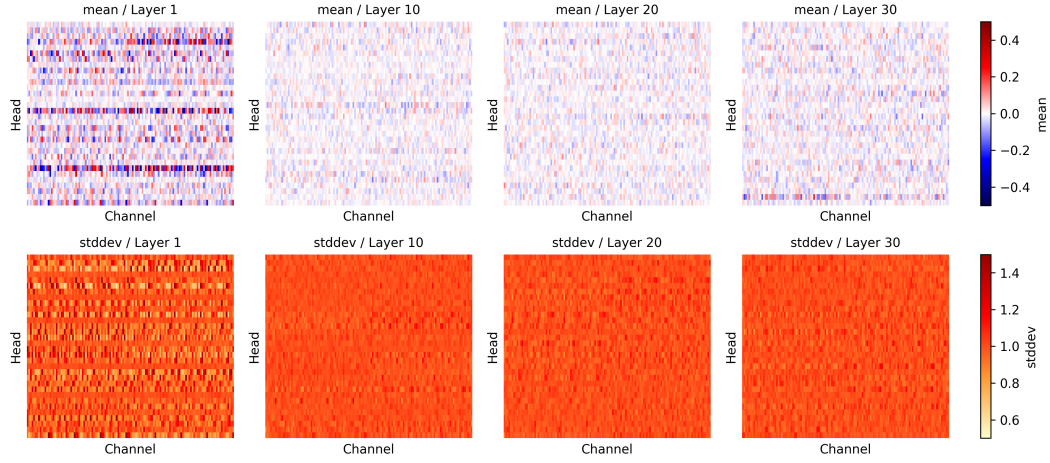
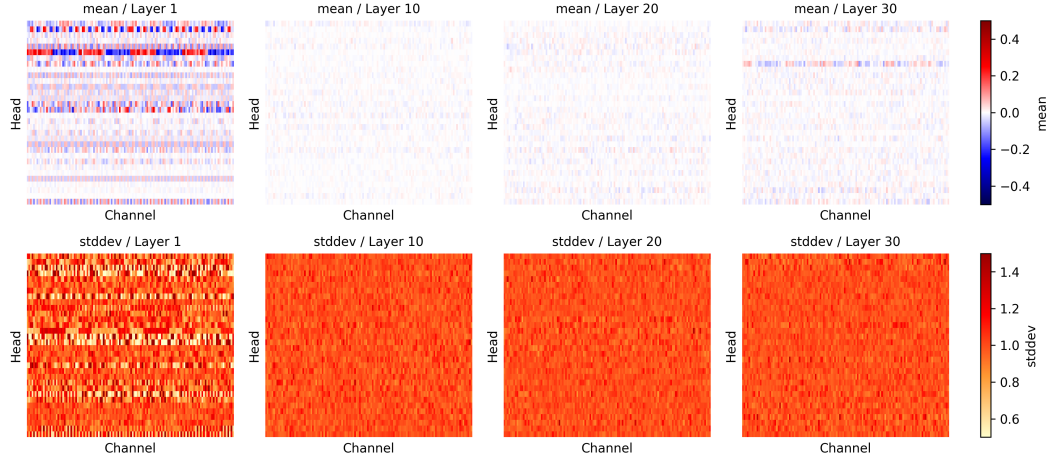


Figure 12: Visualizations of channel-wise mean and standard deviation of **keys** after applying NSN and Hadamard transform to LLaMA2-7B on WikiText-2 (top) and C4 (bottom). The first sample from the test split of each dataset is used for visualization. While NSN overall performs standardization fairly well, it struggles in certain heads of the early layers.

Channel-wise mean / stddev on WikiText-2



Channel-wise mean / stddev on C4

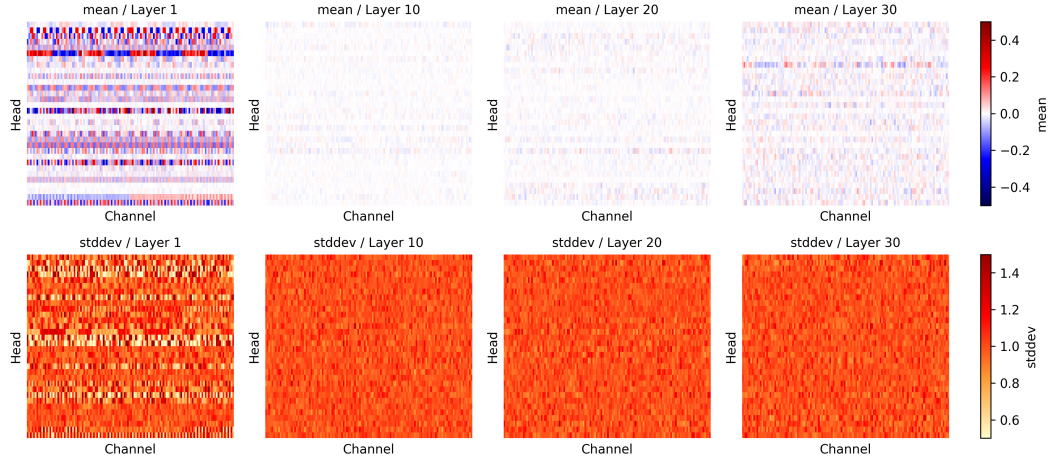


Figure 13: Visualizations of channel-wise mean and standard deviation of **values** after applying NSN and Hadamard transform to LLaMA2-7B on WikiText-2 (top) and C4 (bottom). The first sample from the test split of each dataset is used for visualization. While NSN overall performs standardization fairly well, it struggles in certain heads of the early layers.